(4)

David Taylor Research Center
Bethesda, MD 20084-5000

AD-A202 424

DTRC SHD-1229-01
November 1988

POTENTIAL FLOW EVALUATION OF THE INTERFERENCE EFFECT OF STRUT-THROUGH-APPENDAGE-TIP MODEL MOUNTING TECHNIQUE AND REDUCTION OF THE EFFECT USING BLOWING AND SUCTION

By

Robert W. Mellish
David W. Coder

NOVEMBER 1988
POTENTIAL FLOW EVALUATION OF THE INTERFERENCE EFFECT OF STRUT-THROUGH-APPENDAGE-TIP MODEL MOUNTING TECHNIQUE AND REDUCTION OF THE EFFECT USING BLOWING AND SUCTION
DTRC SHD-1229-01

MAJOR DTRC TECHNICAL COMPONENTS

CODE 011 DIRECTOR OF TECHNOLOGY, PLANS AND ASSESSMENT

12 SHIP SYSTEMS INTEGRATION DEPARTMENT

14 SHIP ELECTROMAGNETIC SIGNATURES DEPARTMENT

15 SHIP HYDROMECHANICS DEPARTMENT

16 AVIATION DEPARTMENT

17 SHIP STRUCTURES AND PROTECTION DEPARTMENT

18 COMPUTATION, MATHEMATICS & LOGISTICS DEPARTMENT

19 SHIP ACOUSTICS DEPARTMENT

27 PROPULSION AND AUXILIARY SYSTEMS DEPARTMENT

28 SHIP MATERIALS ENGINEERING DEPARTMENT

DTRC ISSUES THREE TYPES OF REPORTS:

1. **DTRC reports, a formal series,** contain information of permanent technical value. They carry a consecutive numerical identification regardless of their classification or the originating department.

2. **Departmental reports, a semiformal series,** contain information of a preliminary, temporary, or proprietary nature or of limited interest or significance. They carry a departmental alphanumerical identification.

3. **Technical memoranda, an informal series,** contain technical documentation of limited use and interest. They are primarily working papers intended for internal use. They carry an identifying number which indicates their type and the numerical code of the originating department. Any distribution outside DTRC must be approved by the head of the originating department on a case-by-case basis.

UNCLASSIFIED
SECURITY CLASSIFICATION OF THIS PAGE

AD-A202 424

REPORT DOCUMENTATION PAGE

1a. REPORT SECURITY CLASSIFICATION UNCLASSIFIED	1b. RESTRICTIVE MARKINGS
2a. SECURITY CLASSIFICATION AUTHORITY	3. DISTRIBUTION/AVAILABILITY OF REPORT Approved for public release; distribution is unlimited.
2b. DECLASSIFICATION/DOWNGRADING SCHEDULE	
4. PERFORMING ORGANIZATION REPORT NUMBER(S) DTNSRDC-SPD 1229-01	5. MONITORING ORGANIZATION REPORT NUMBER(S)
6a. NAME OF PERFORMING ORGANIZATION David Taylor Naval Ship R&D Center 6b. OFFICE SYMBOL (If applicable) Code 1543	7a. NAME OF MONITORING ORGANIZATION
6c. ADDRESS (City, State, and ZIP Code) Bethesda, Maryland 20084-5000	7b. ADDRESS (City, State, and ZIP Code)
8a. NAME OF FUNDING/SPONSORING ORGANIZATION ONT 8b. OFFICE SYMBOL (If applicable)	9. PROCUREMENT INSTRUMENT IDENTIFICATION NUMBER
8c. ADDRESS (City, State, and ZIP Code)	10. SOURCE OF FUNDING NUMBERS PROGRAM ELEMENT NO. / PROJECT NO. / TASK NO. / WORK UNIT ACCESSION NO. DN378001

11. TITLE (Include Security Classification)
Potential Flow Evaluation of the Interference Effect of Strut-Through-Appendage-Tip Model Mounting Technique and Reduction of the Effect Using Blowing and Suction.

12. PERSONAL AUTHOR(S)
Mellish, R. W., and D. W. Coder

13a. TYPE OF REPORT	13b. TIME COVERED	14. DATE OF REPORT (Year, Month, Day)	15. PAGE COUNT
Departmental	FROM _____ TO _____	March 1987	69

16. SUPPLEMENTARY NOTATION

17. COSATI CODES		
FIELD	GROUP	SUB-GROUP

18. SUBJECT TERMS (Continue on reverse if necessary and identify by block number)
Strut Interference, Blowing, and suction, (Augm)
Model Mounting Techiques,
Potential Flow

19. ABSTRACT (Continue on reverse if necessary and identify by block number)

A parametric study based on incompressible, irrotational flow theory was conducted to evaluate the effect of strut support interference on the flow field about a model. The use of suction and blowing to correct the support interference is also investigated. Two struts were considered for numerical analysis, a small chord strut of constant cross section and a large chord strut of varying cross section, both attached to the tip of a model submarine sail. For the present study the SS N21 class and SSN 688 class sail geometries are utilized.

To assess the level of strut interference, the pressure fields on the surface of the sail and a flat plate representation of the hull were evaluated as follows. The flow field was computed for the model geometry without a strut attached (baseline configuration) and the results are compared with identical calculations for the model-

(Continued on reverse side)

20. DISTRIBUTION/AVAILABILITY OF ABSTRACT	21. ABSTRACT SECURITY CLASSIFICATION
☐ UNCLASSIFIED/UNLIMITED ☐ SAME AS RPT. ☐ DTIC USERS	UNCLASSIFIED
22a. NAME OF RESPONSIBLE INDIVIDUAL Robert W. Mellish	22b. TELEPHONE (Include Area Code) 202-227-1326 / 22c. OFFICE SYMBOL Code 1543

DD FORM 1473, 84 MAR — 83 APR edition may be used until exhausted. All other editions are obsolete.

SECURITY CLASSIFICATION OF THIS PAGE

(Block 19 continued)

cont'd

delta

strut combination. The calculated results are presented graphically as contour plots of the pressure coefficient (C_p^n). Contour plots of δC_p^n (the difference between baseline and sail-strut results) are utilized to identify regions of principal strut interference. Finally, suction and blowing was applied to minimize strut interference in areas considered important to hull boundary layer and sail flow that would affect wake measurments.

Keywords:

CONTENTS

FIGURES

FIGURES (Continued)

ABSTRACT

A parametric study based on incompressible, irrotational flow theory was conducted to evaluate the effect of strut support interference on the flow field about a model. The use of suction and blowing to correct the support interference is also investigated. Two struts were considered for numerical analysis, a small chord strut of constant cross section and a large chord strut of varying cross section, both attached to the tip of a model submarine sail. For the present study the SSN 21 class and SSN 688 class sail geometries are utilized.

To assess the level of strut interference, the pressure fields on the surface of the sail and a flat plate representation of the hull were evaluated as follows. The flow field was computed for the model geometry without a strut attached (baseline configuration) and the results are compared with identical calculations for the model-strut combination. The calculated results are presented graphically as contour plots of the pressure coefficient C_p. Contour plots of ΔC_p (the difference between baseline and sail-strut results) are utilized to identify regions of principal strut interference. Finally, suction and blowing was applied to minimize strut interference in areas considered important to hull boundary layer and sail flow that would affect wake measurements.

ADMINISTRATIVE INFORMATION

This work was sponsored by the Office of Naval Technology 6.2 Propulsor Subproject (1-1540-005)

INTRODUCTION

Experiments conducted in the Anechoic Flow Facility (AFF) at the David Taylor Naval Ship Research and Development Center (DTNSRDC) that investigate flow phenomena associated with submarine geometries have necessitated the use of mounting arrangements of the type illustrated by Fig. 1. Qualitative studies of strut interference effects utilizing a 1/32 scale SSN 688 model employing oil drop and oil film flow visualization techniques have been conducted to investigate the

general character of the flow in the area of the sail. Analysis of the topology of skin friction lines (Lighthill[1])* on the sail lead to the conclusion that the presence of the strut significantly alters the pattern of three dimensional separation on the sail cap and the area immediately forward of the sail trailing edge. It is presumed the altered separation patterns found are the result of changes in the pressure distribution about the sail due to the strut, and would significantly affect the hull boundary layer at the root of the sail, eventually influencing the circumferential harmonic content of the model propulsor time-averaged velocity inflow.

The eventual use of the present study is to determine ways to improve model wake measurements by minimizing strut interference in general and specifically for two struts currently in use at the AFF. Since the pressure field established by the external flow plays a significant role in the onset of separation, specific attention was given to the alteration of this flow parameter by the strut. Thus strut interference as presented by this report utilizes a comparative method. The perturbation of the pressure field produced by the strut is assumed to be the difference between the pressure fields produced by the model with and without the strut present.

Two sail-strut combinations are utilized for the numerical analysis. The first combination considered is the SSN 21 sail coupled to a strut of streamline shape and constant cross section (commercially available material). Overall, this strut has a chord of 4.0 in. and a maximum thickness of 1.7 in. The second combination is the SSN 688 sail mated to a strut comprised of two dissimilar shapes. Mounted to the floor of the wind tunnel facility is a large streamline foil shape 30 in. in height whose chord varies linearly from 22.5 in. to 18 in.

---

*References are to be found on page 69.

near the model. Spanning the remaining distance to the model is a solid rectangular sting-strut 3.0 in. wide and 3.4 in. long. Both struts are currently available for use at the AFF.

Because of the difference in physical size and shape of the two struts described above, each presents a very different level of flow interference and structural strength and rigidity. The smaller strut produces less interference to the flow but is not as strong or rigid as the larger strut. Thus, the smaller strut is adapted whenever the model mounting requirements will accept it. However, there are many situations that demand the strength and rigidity of the larger strut. Because of its large interference effects, the larger strut was selected as the primary test case. The rationale is that if it were possible to reduce the large strut's adverse interference effects, the smaller strut's adverse interference effects would be as easy to handle. Therefore, the application of suction and blowing is evaluated as a device to improve the flow for the large strut.

NUMERICAL PROCEDURE

The displacement of the freestream flow by the body is modeled by a Rankine source panel method first developed by Hess and Smith[2]. In this method, the body is descretized by flat four sided panels. In the plane of each quadrilateral resides a surface singularity (source or sink) of unspecified magnitude. The application of the Neumann boundary condition to each panel results in a matrix equation in terms of the unknown source strengths. The source strengths are solved numerically and the flow field is thus fully determined.

In order to save computer and manpower time, an approximation of the physical model was implemented utilizing the sail or sail-strut combination mounted on an

infinite flat plate in an unbounded, inviscid, and irrotational fluid. Since a comparative method is used, the important differences in pressure fields will be due to the inclusion of the strut and discrepancies with the potential flow model will not be too important. If it were desirable to fully represent the model mounted in the wind tunnel facility as accurately as possible, the demands for storage would rapidly become large. Inclusion of tunnel walls by the method of images or by panel distributions of finite span would be a logical next step of improved representation of the facility; see Holt[3].

The procedure for comparing the interference effects of the strut geometries is given below. The body under consideration was discretized by plane quadrilateral elements. The maximum number of elements was kept below 900, the limit for an expanded version of the computer code used as described in reference 4. The primary characteristic of the discretized representation of the models which have an effect on the computed results are panel size and distribution. Panels were concentrated in areas where flow properties were expected to vary rapidly and were spread out where the gradients were expected to be small. The results of the paneling efforts are presented in Fig. 2 through Fig. 8.

The discretized SSN 21 sail used for the baseline (no strut) calculations is shown in Fig. 2. Evident from this figure are the characteristics discussed above. Fig. 3 shows the SSN 21 sail with the small strut. Together these two geometries are used for the first case discussed in the following section. Figures 4, 5 and 6 are the paneled representations of the SSN 688 sail without sailplanes, SSN 688 sail without sailplanes coupled to the large strut and a closeup of the sting-strut for the SSN 688 sail strut combination, respectively. For most of the study, the SSN 688 sail is used without planes.

To verify that the resolution of the panel distribution was adequate, the SSN 688 sail was discretized using 876 and 692 panels and the resulting, computed source distributions were compared. The input geometries for the 876 case is presented by Fig. 7 and the 692 case by Fig. 8. The resulting source distributions are presented by Figs. 9 and 10. Since the source distributions are essentially identical, the 692 panel model is considered adequate.

The figures presented above represent the complete set of geometries utilized by the parametric study presented by this report. The x, y and z ordered triplet of point data plus specifiers of line and section number constitutes the numerical geometry input for the potential flow program. After choosing planes of symmetry and input/output options the XYZPF[4] program was executed and the resulting flow computed. Suction and blowing are specified by panel number and source strength. For all figures presented in this report, the direction of the onset flow is from left to right.

For the baseline configuration of the sail alone, the numerical results are used to produce contour plots on the sail of nondimensional pressure coefficient,

$$C_p = \frac{P - P_\infty}{\frac{1}{2}\rho U^2} \qquad [1]$$

where

P = pressure

P_∞ = pressure at infinity

ρ = fluid density, and

U = free stream velocity.

The strut of finite length is added to the sail geometry and the potential flow calculations are repeated. By comparing the C_p contours on the sail for both

geometries the effect of the strut is revealed. To illustrate the comparison of baseline vs. sail-strut graphically, contours for ΔC_p ($C_{p_{strut}}-C_{p_{baseline}}$) are also presented. Contours of C_p and ΔC_p for the area in front of the sail on the flat plate representation of the hull are also considered. The region forward of the sail in the junction between the hull and the sail is important to the formation of three dimensional separation typified by a vortex that bends around the sail base. This area of separation is perhaps more important to the propulsor inflow than the sail separation.

RESULTS AND DISCUSSION

The order of the presentation of the computed results is as follows. The SSN 21 sail with the small strut is presented first followed by the SSN 688 sail with the large strut. This latter case includes suction and blowing.

The coefficient of pressure for the SSN 21 sail with and without the small strut attached are presented by Figures 11a and 11b. Contours of C_p for the baseline configuration (sail only) are given by Fig. 11a and the associated contour levels are tabulated on the same page. Values of C_p vary from 1.0 at the leading edge stagnation to approximately 0.2 near the trailing edge. As expected, this figure illustrates an intense negative pressure gradient over the nose radius and the acceleration the flow to a C_p of approximately -0.5 in the region of 1/8 chord. As given by Figure 11a, aft of the 1/8 chord position is a large area with a small adverse pressure gradient (defined as a positive gradient in the direction of flow), that leads to a value of about C_p=0.2 at the trailing edge. Three dimensional influences are evident by the bending of contours beginning at around the mid-height region and extending to the cap. The addition of the small strut results in the contours of pressure coefficient given by Fig. 11b. Similar

features to those noted above are evident by this figure, the only exception being the additional pressure gradients in the area adjacent to the strut. The addition of the strut impacts the pressure field as clearly illustrated by Fig. 11c; the ΔC_p contours. An important result is the identification of a large area of unperturbed flow. Even the highest difference noted is a value of ΔC_p=-0.175. The result and conclusions are similar for the area immediately forward of the sail on the flat plate representation of the of the model. Figures 11d, 11e and 11f show very small levels of disturbance due to the addition of the strut. In summary, based on the above observations, we conclude that the small strut used in the analysis presents a low level of interference and is a minimum interference choice for model support during wake measurements. An additional question not addressed here is the degree of structural rigidity required which could present difficulties for the small strut. The second, more structurally robust, large strut is considered below.

After reviewing the computed results for the SSN 688 sail with fairwater planes (not presented), with and without the large AFF strut, the decision was made to simplify the geometry by removing the planes. Thus, for the discussion which follows, reference to the SSN 688 sail will indicate the representation without sailplanes.

Figure 12 presents the C_p contours for the baseline configuration, namely the SSN 688 sail without the large strut present. The characteristics of the pressure field produced by this geometry are consistent and closely parallel those of the baseline SSN 21 case discussed previously (this is to be expected since the bodies are similar). A compact area of favorable pressure gradient rapidly evolves into a large area of adverse pressure gradient which is three dimensional near the sail cap. The significant difference between the SSN 21 sail (Fig. 11a) and the SSN 688 sail (Fig. 12a) is that the levels of C_p attained over the body are lower for the

latter. The addition of the large strut produces a radical change of the pressure contours as depicted by Fig. 12b. Salient features are a reduction of three dimensional end cap effects, a more accelerated flow over the sail nose, a sail mid-body of fairly constant pressure followed by a more spatially compact area of retarded flow. The ΔC_p given in Figure 12c illustrates the area of fluid velocity affected by the presence of the strut. The majority of the sail surface is influenced by the strut corresponding to a ΔC_p value of -0.08 which decreases gradually as the strut intersection point is approached. On the after part of the sail we see that the adverse pressure gradient is reduced.

For the area forward of the sail, on the flat plate ship's hull, we refer to Fig. 12d, 12e and 12f. The figures reveal that the effects of the strut are not severe due to the large distance of the area from the strut.

The potential flow code was modified to add the suction and blowing boundary conditions and the resulting executable version was verified using a sphere test case. To discuss the results for the cases involving suction and blowing as applied to the large strut it is first necessary to understand the sectional scheme used to delineate the geometry. With reference to Figures 5 and 6, one may logically divide the input geometry into five main sections; namely, from top to bottom, the strut, strut cap, sting, sail cap and the sail. The discussion which follows presents the results of suction and blowing applied to the sections defined above in various combinations and with various strengths.

The first case considered is an effort designed to negate the source strength of the strut, strut cap and sting through application of the appropriate suction and blowing boundary condition. To achieve this goal the required strength of the volume flux at each panel as specified by the additional suction or blowing boundary condition must be equal to 2π times the computed source strength required

to satisfy the Neumann condition (i.e. two dimensional sink or source singularity). This is precisely the source strength given by the basic potential flow calculation. Results of these calculations are given by Figures 13, 13b and 13c which depict the on body streamlines, pressure coefficient contours for the sail-strut combination and the ΔC_p contours for the strut-baseline difference. As is evident from this series of figures the negation of the source or sink contribution to the flow of the entire strut nearly restores the baseline results. The -0.08 ΔC_p level which was found to exist near the leading and trailing edges of the sail for the uncorrected case is now present only a small distance from the sail-strut intersection. This very favorable result is also evidenced by Figures 13d and 13e for the area forward of the sail. The flow rates required to produce the cancellation of the strut appear to be practical when applied by a 4-in. pipe and applying the limiting factors of choked flow for air and cavitation for water.

To qualify the effectiveness of the negation of the source strength of the panels further, suction and blowing was applied to the strut section alone. The resulting streamlines, C_p contours and ΔC_p contours for the sail, negating the top strut section only, are given by Fig. 14a, Fig. 14b and Fig. 14c, respectively. The corresponding figures for the hull surface forward of the sail are presented by Figures 14d and 14e. This case is, of course, less effective but is the major contributor to the previously discussed results due to the percentage of surface area represented by this section. The strut section also has the advantage of its size making it a candidate for installation of the required hardware to actually implement the results found.

The combination of suction and blowing was only considered for the topmost strut section due to its remote position to the sail. The other sections are considered too close to the sail for the application of blowing based on a concern

that other deleterious effects could be prompted; such as additional areas of separated flow. Therefore, for the other sections of the model, suction only was applied.

Discussed next are the results of suction applied to the strut, strut cap and sail cap. The intensity of the suction is that required to negate the source panels on the sections mentioned above. The figures pertaining to this subject are Fig. 15a through Fig. 17e. Analysis of the contours for the sail pressure distribution illustrate that suction applied in proportion to the source panel is effective to a limited degree if the resulting volume flow of the applied suction is small. Although the volume flow of the suction is more effective the closer the proximity to the point of interest. Because of the large surface area of the strut section the resulting volume flow of the applied suction is 20 times that of the strut cap section and 200 times that of the sail cap section. However the correction produced by suction applied to the strut section is considerable when compared to the results obtained from the strut and sail cap sections which are negligible. Effectiveness of the suction for the flat plate hull surface is minimal due to the displacement of the applied sinks; this applies to all three cases.

The final application of suction is an attempt to apply the total volume flow which most nearly negated the influence of the strut section to the strut and sail cap sections. The two sections indicated above are reasonable choices for an actual installation and their proximity to the sail body where it is desired to correct the strut interference is considered advantageous.

Results for the data obtained are given by Figures 18a through 19e. For both the sail and hull areas the correction for strut effects is excessive and grossly distorts the flow. The streamlines in particular illustrate the migration of fluid

toward the concentrated sink effect of the suction. Since the volume flow of this case is too extreme, the optimum solution appears to lie between this case and the others discussed previously.

CONCLUSION AND RECOMMENDATIONS

Conclusions:

(1) The application of potential flow code to evaluate the qualitative effects of strut interference is, in general, a useful and effective tool.

(2) Where strut interference is considered excessive suction and blowing may provide a mechanism for improving the disturbed flow.

(3) Sensitivity of the pressure field to the suction flow rate is not considered excessive for the practical use of suction in a flow facility.

Recommendations:

(1) An experimental procedure should be developed to verify the results found and the resulting methodology be tested under experimental test conditions.

(2) Wall effects in the panel method should be included to better model the actual test facility.

ACKNOWLEDGMENTS

The authors also acknowledge the invaluable assistance provided by code 1843, specifically B. H. Cheng and R. W. Miller, with regard to the execution of the computer program and the preparation of the figures.

Fig. 1. Typical model support in wind tunnel viewing downstream

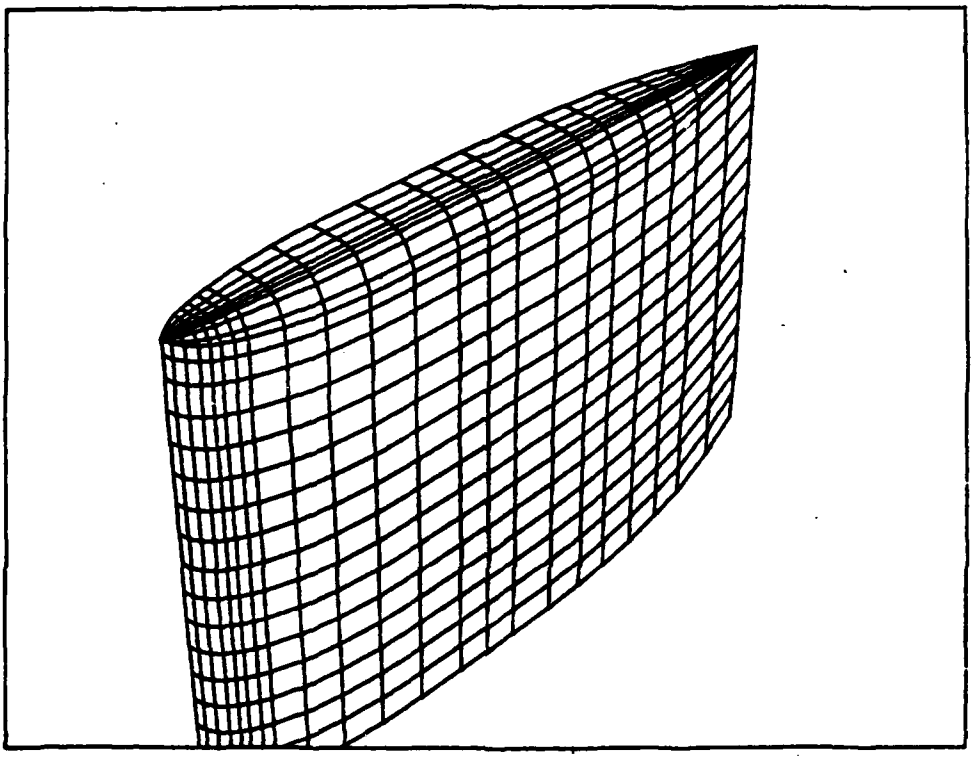

Fig. 2. SSN 21 sail.

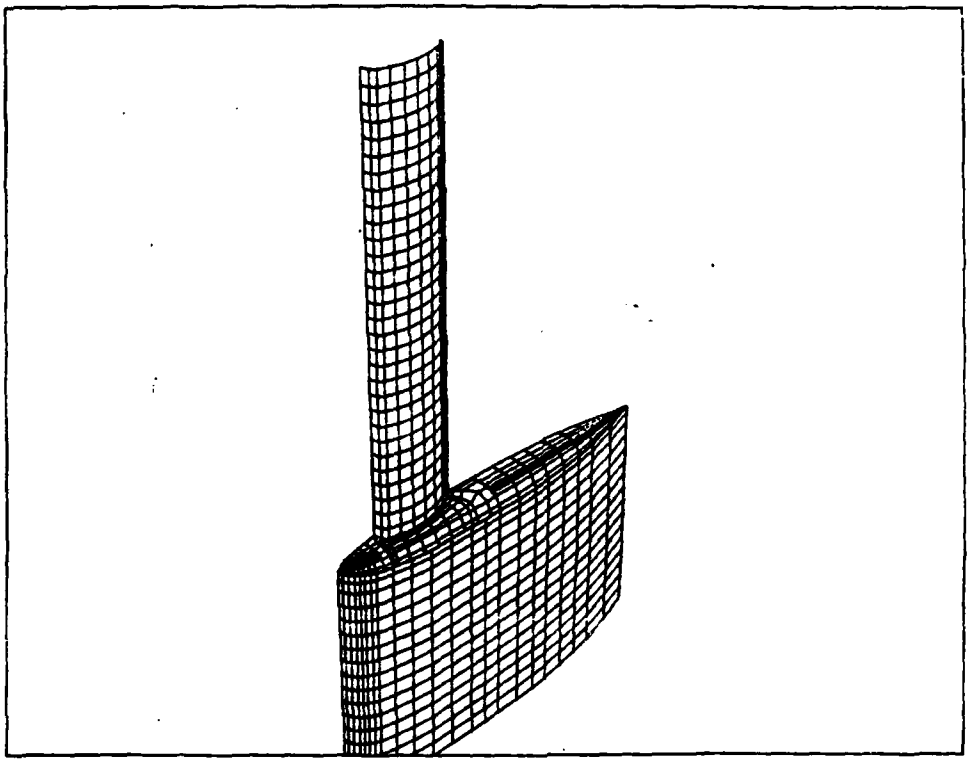

Fig. 3. SSN 21 sail with small strut.

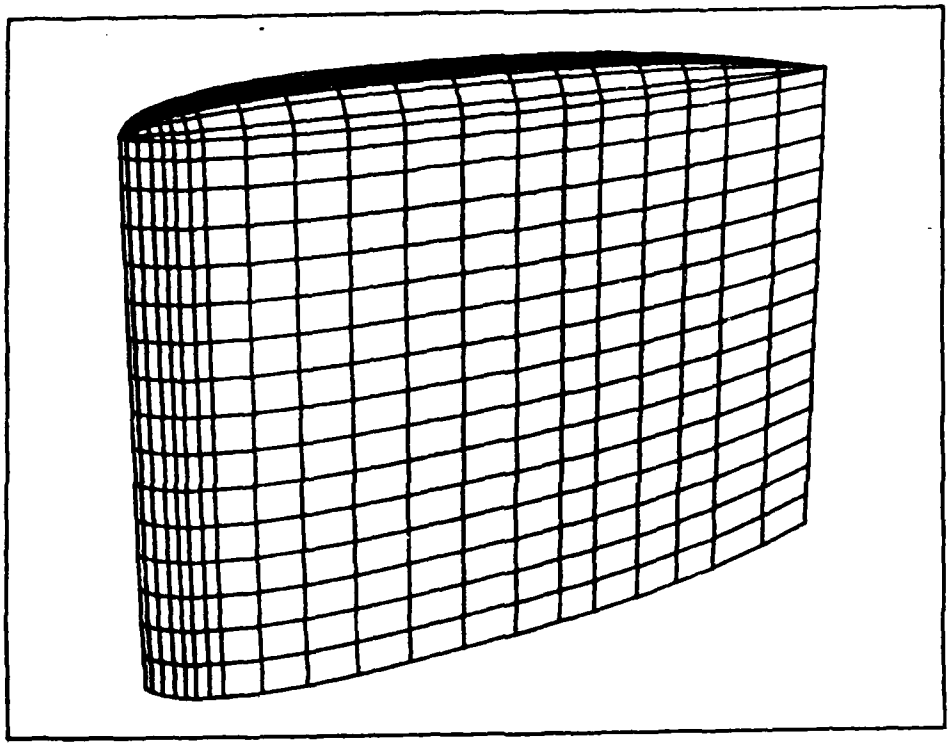

Fig. 4. SSN 688 sail without fairwater planes.

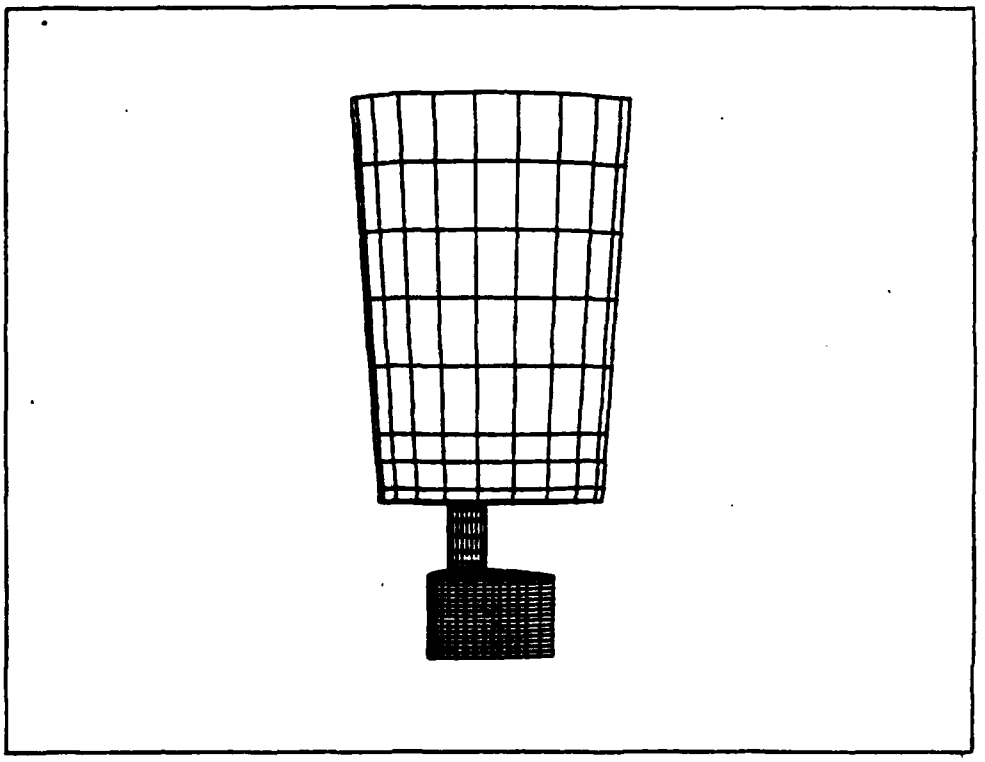

Fig. 5. SSN 688 sail with large strut and without fairwater planes.

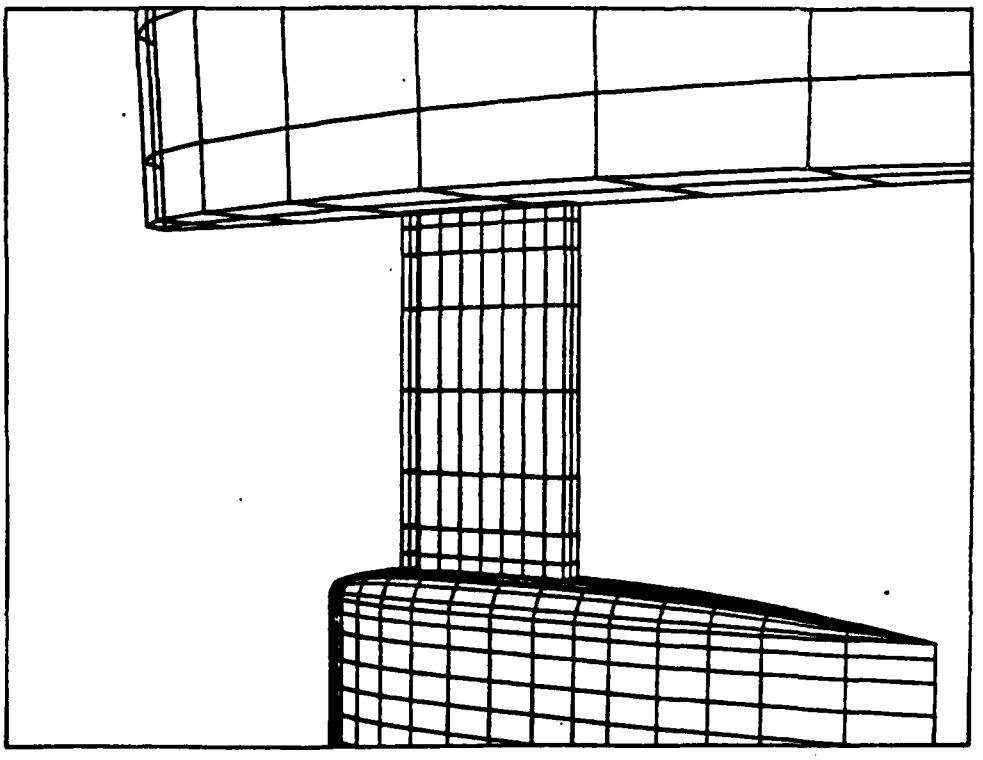

Fig. 6. Closeup of SSN 688 sail, cap, sting-strut, and large strut end cap.

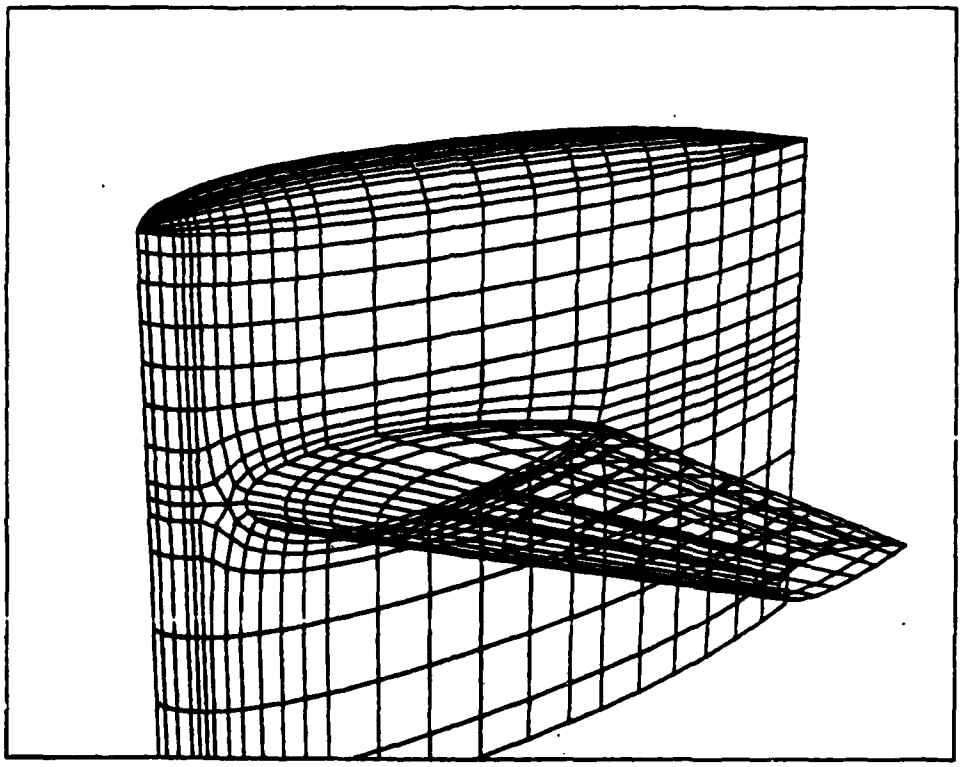

Fig. 7. 867 panel representation of the SSN 688 sail with fairwater planes.

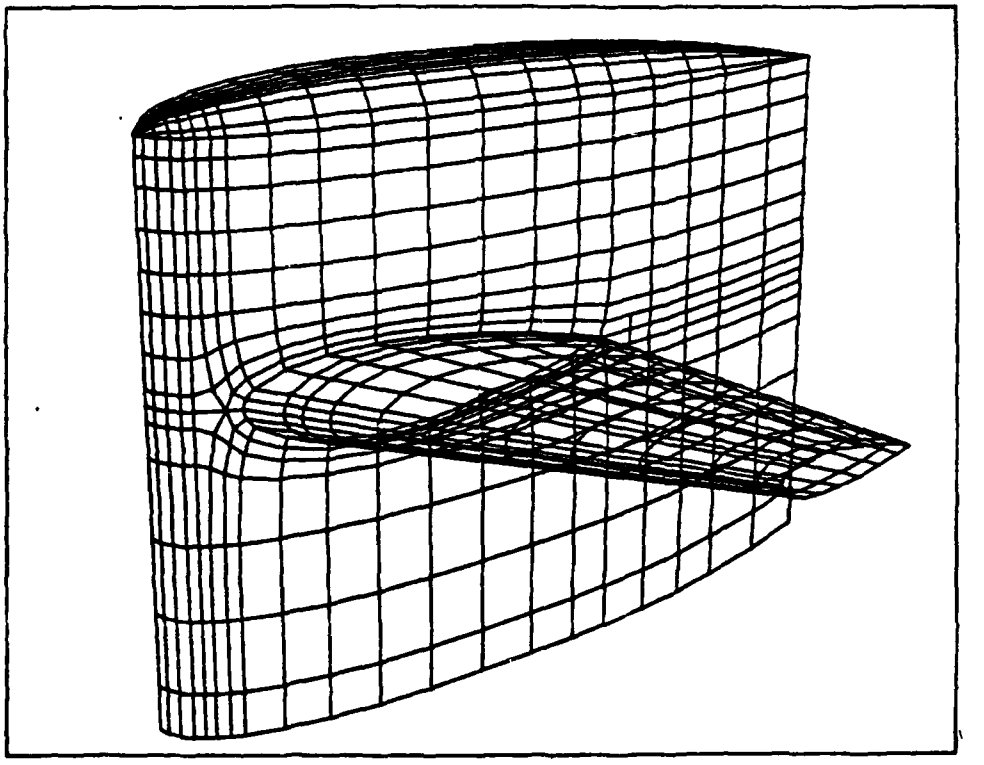

Fig. 8. 692 panel representation of the SSN 688 sail with fairwater planes.

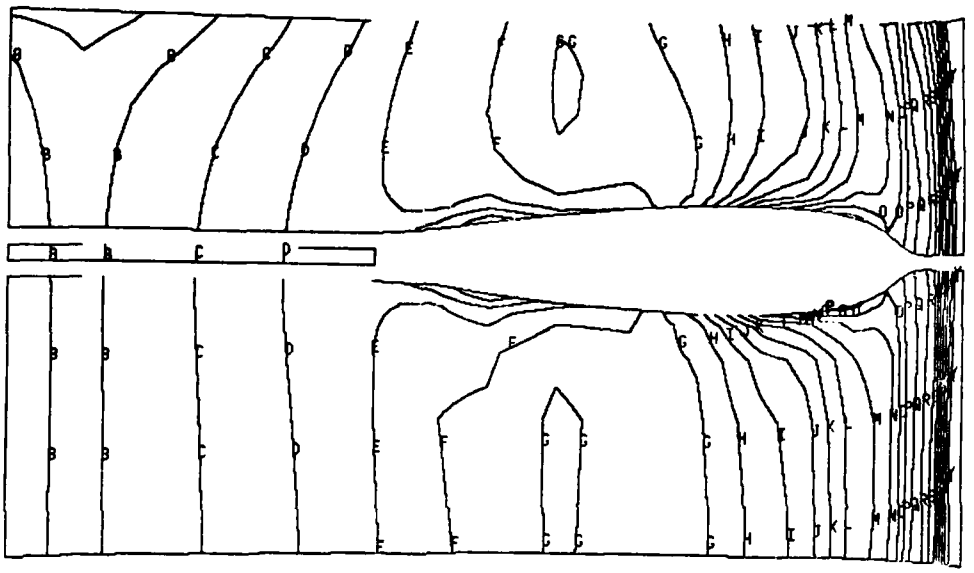

Fig. 9. 876 panel source distribution.

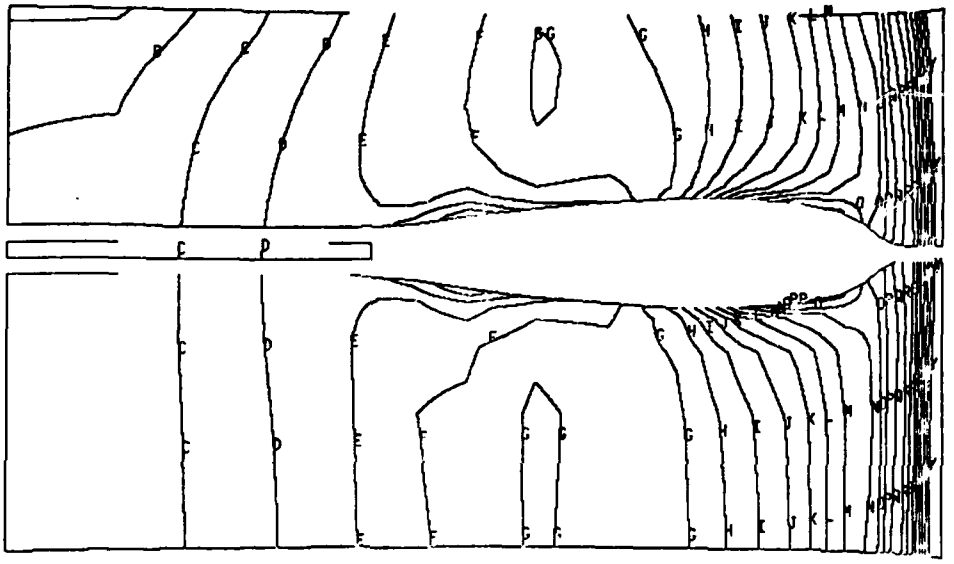

Fig. 10. 692 panel source distribution.

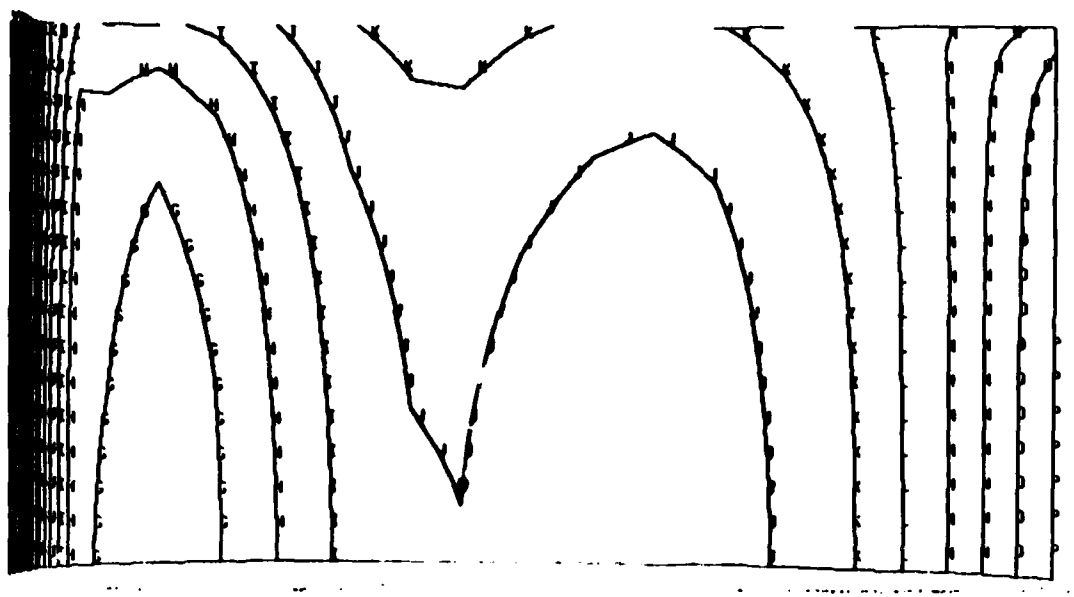

Fig. 11a. C_p contours on the sail surface, sail without strut.

Fig. 11. Pressure contours for the SSN 21.

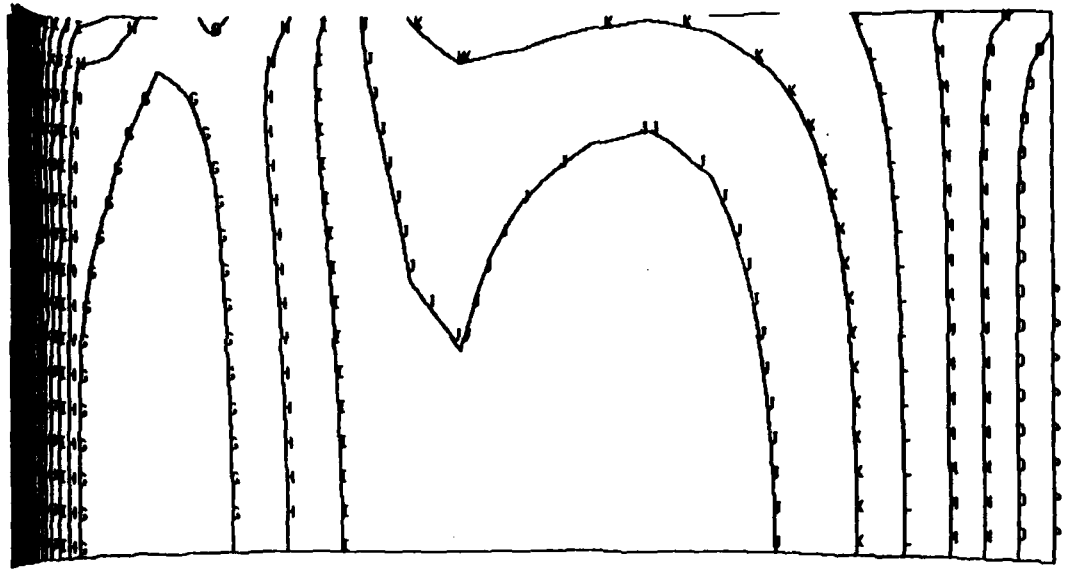

Fig. 11b. C_p contours on the sail surface, sail with small strut.

Fig. 11. (Continued)

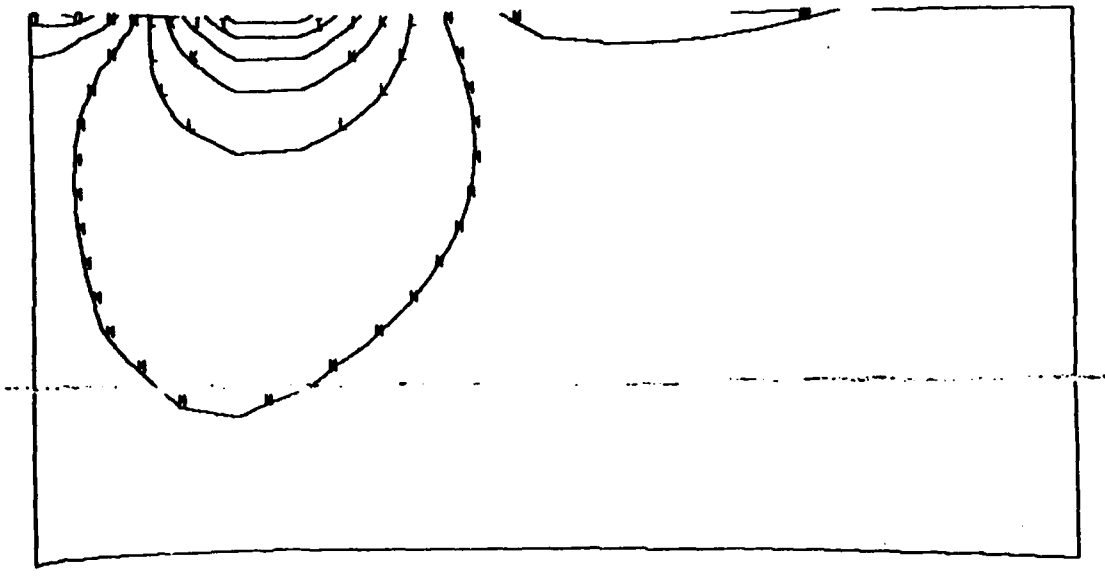

<a = -0.400>
<b = -0.368>
<c = -0.336>
<d = -0.304>
<e = -0.272>
<f = -0.240>
<g = -0.208>
<h = -0.176>
<i = -0.144>
<j = -0.112>
<k = -0.080>
<l = -0.048>
<m = -0.016>
<n = 0.016>
<o = 0.048>
<p = 0.060>
<q = 0.112>
<r = 0.144>
<s = 0.176>
<t = 0.208>
<u = 0.240>
<v = 0.272>
<w = 0.304>
<x = 0.336>
<y = 0.368>
<z = 0.400>

Fig. 11c. ΔC_p contours on the sail surface.

Fig. 11. (Continued)

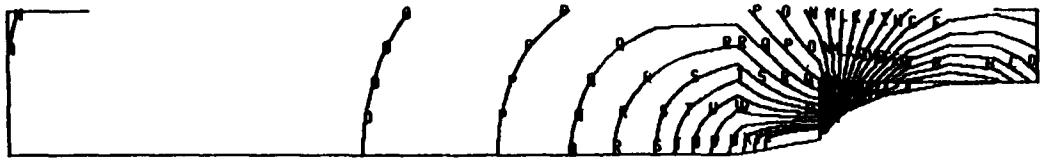

Fig. 11d. C_p contours on the hull surface, sail without strut.

Fig. 11. (Continued)

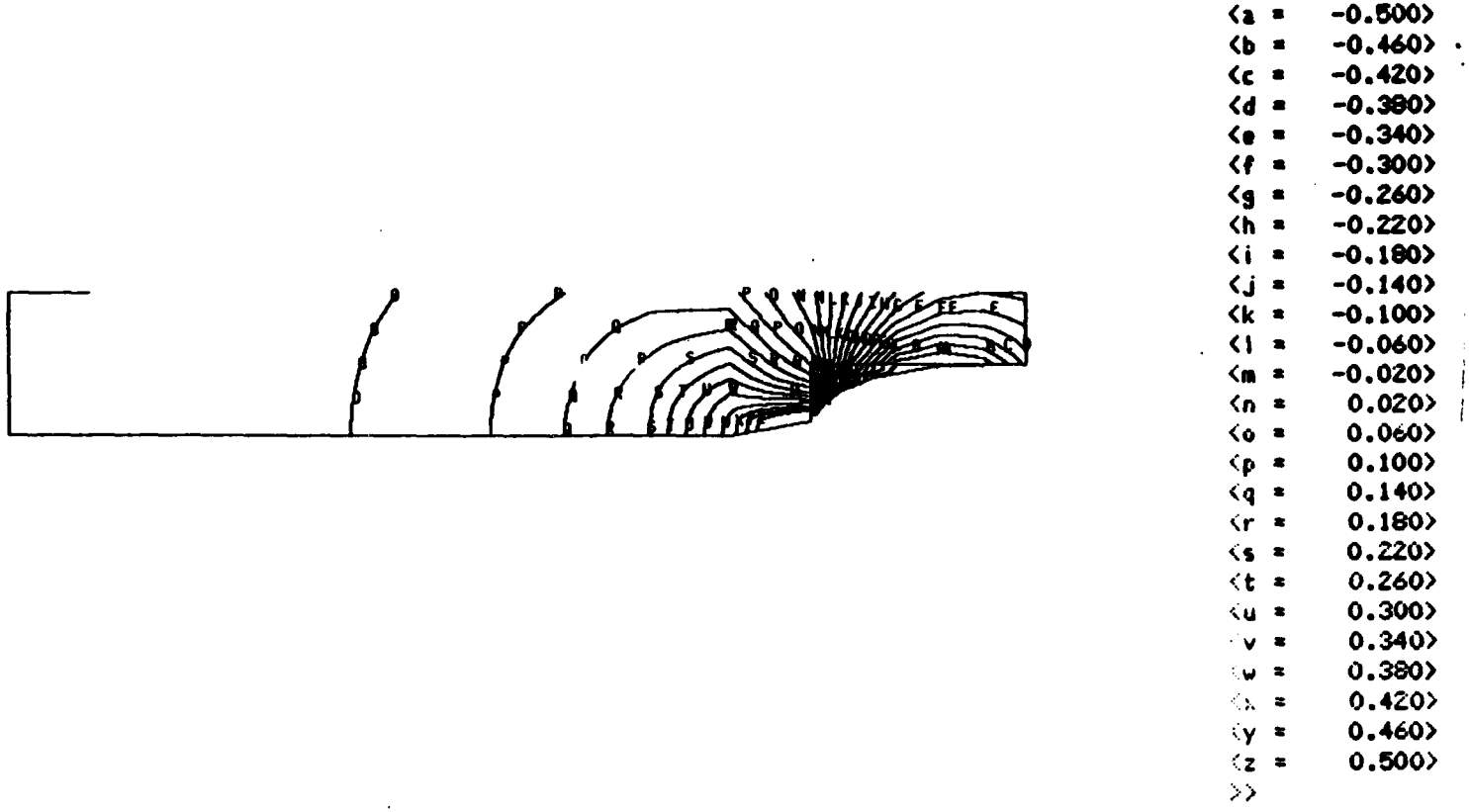

Fig. 11e. C_p contours on the hull surface, sail with small strut.

Fig. 11. (Continued)

<a = -0.200>
<b = -0.184>
<c = -0.168>
<d = -0.152>
<e = -0.136>
<f = -0.120>
<g = -0.104>
<h = -0.088>
<i = -0.072>
<j = -0.056>
<k = -0.040>
<l = -0.024>
<m = -0.008>
<n = 0.008>
<o = 0.024>
<p = 0.040>
<q = 0.056>
<r = 0.072>
<s = 0.088>
<t = 0.104>
<u = 0.120>
<v = 0.136>
<w = 0.152>
<x = 0.168>
<y = 0.184>
<z = 0.200>
>>

Fig. 11f. ΔC_p contours on the hull surface.

Fig. 11. (Continued)

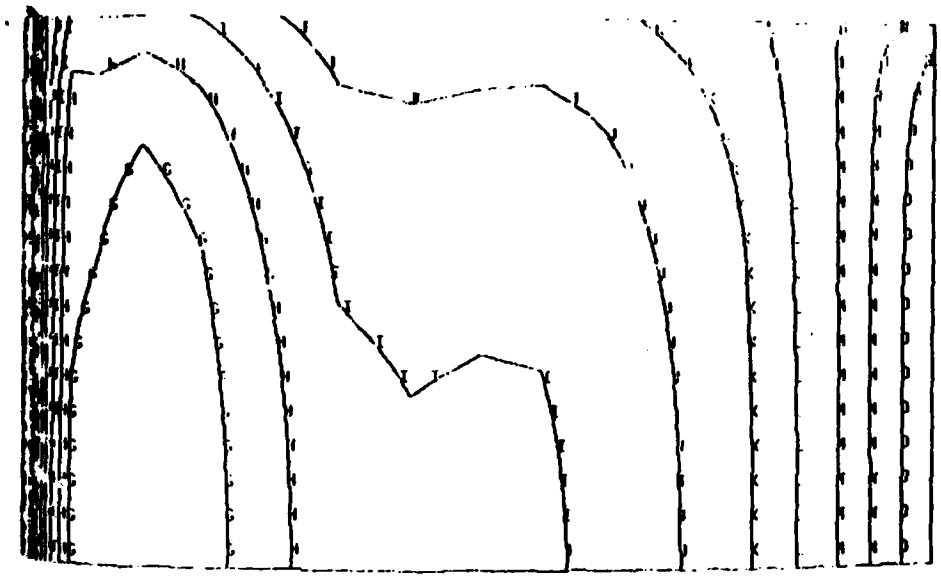

Fig. 12a. C_p contours on the sail surface, sail without strut.

Fig. 12. Pressure contours for the SSN 688.

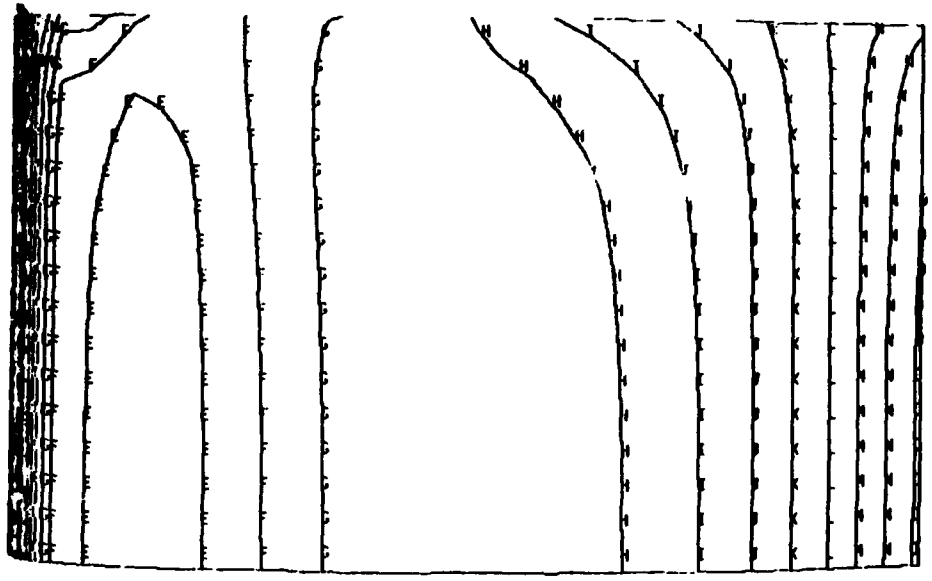

<a = -1.000>
<b = -0.920>
<c = -0.840>
<d = -0.760>
<e = -0.680>
<f = -0.600>
<g = -0.520>
<h = -0.440>
<i = -0.360>
<j = -0.280>
<k = -0.200>
<l = -0.120>
<m = -0.040>
<n = 0.040>
<o = 0.120>
<p = 0.200>
<q = 0.280>
<r = 0.360>
<s = 0.440>
<t = 0.520>
<u = 0.600>
<v = 0.680>
<w = 0.760>
<x = 0.840>
<y = 0.920>
<z = 1.000>

Fig. 12b. C_p contours on the sail surface, sail with large strut.

Fig. 12. (Continued)

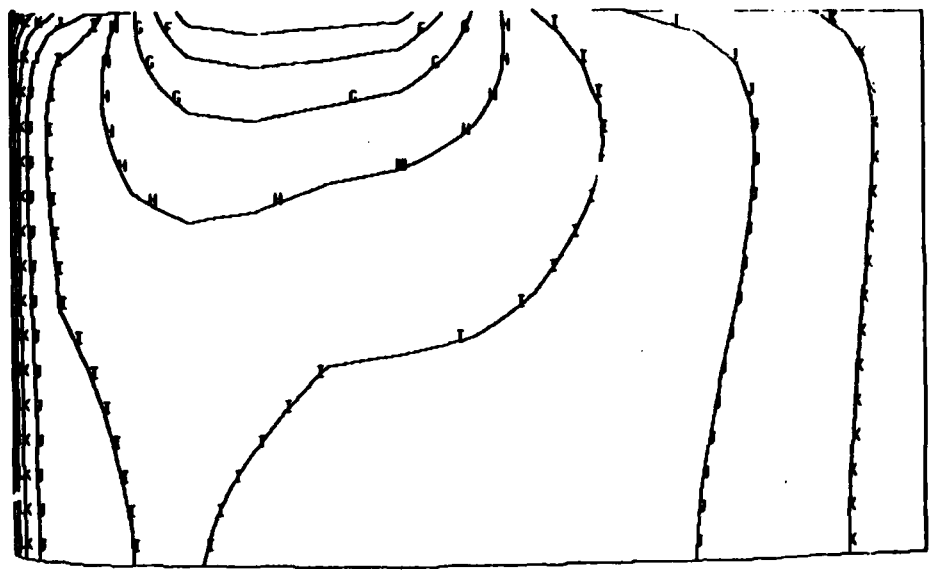

<a = -0.400>
<b = -0.368>
<c = -0.336>
<d = -0.304>
<e = -0.272>
<f = -0.240>
<g = -0.208>
<h = -0.176>
<i = -0.144>
<j = -0.112>
<k = -0.080>
<l = -0.048>
<m = -0.016>
<n = 0.016>
<o = 0.048>
<p = 0.080>
<q = 0.112>
<r = 0.144>
<s = 0.176>
<t = 0.208>
<u = 0.240>
<v = 0.272>
<w = 0.304>
<x = 0.336>
<y = 0.368>
<z = 0.400>

Fig. 12c. ΔC_p contours on the sail surface.

Fig. 12. (Continued)

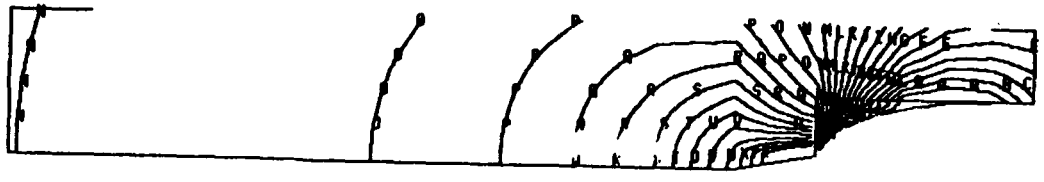

<a = -0.500>
<b = -0.460>
<c = -0.420>
<d = -0.380>
<e = -0.340>
<f = -0.300>
<g = -0.260>
<h = -0.220>
<i = -0.180>
<j = -0.140>
<k = -0.100>
<l = -0.060>
<m = -0.020>
<n = 0.020>
<o = 0.060>
<p = 0.100>
<q = 0.140>
<r = 0.180>
<s = 0.220>
<t = 0.260>
<u = 0.300>
<v = 0.340>
<w = 0.380>
<x = 0.420>
<y = 0.460>
<z = 0.500>

Fig. 12d. C_p contours on the hull surface, sail without strut.

Fig. 12. (Continued)

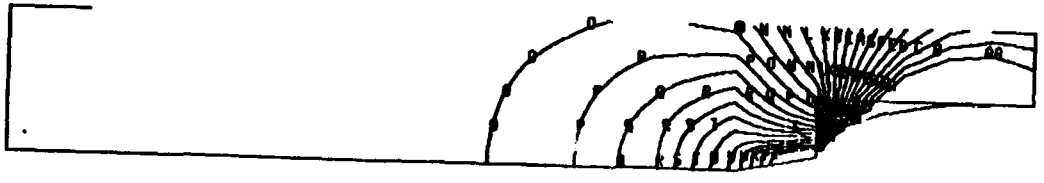

Fig. 12e. C_p contours in the hull surface, sail with large strut.

Fig. 12. (Continued)

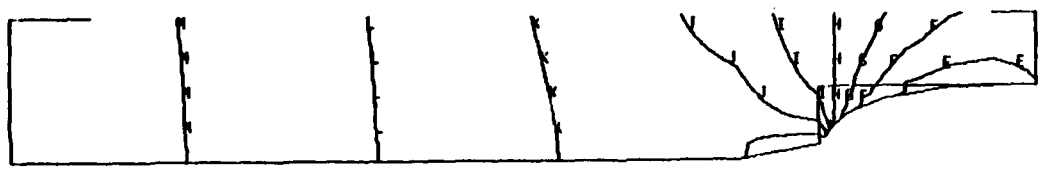

Fig. 12f. ΔC_p contours on the hull surface.

Fig. 12. (Continued)

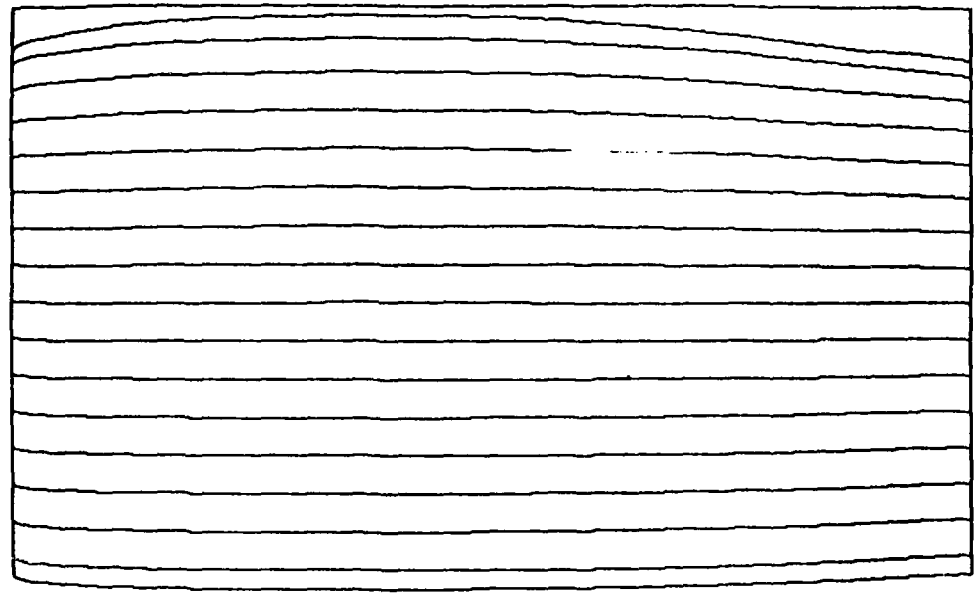

Fig. 13a. Streamlines on the sail surface, sail and large strut.

Fig. 13. Streamlines and pressure contours for the SSN 688 with suction and blowing applied to the entire strut.

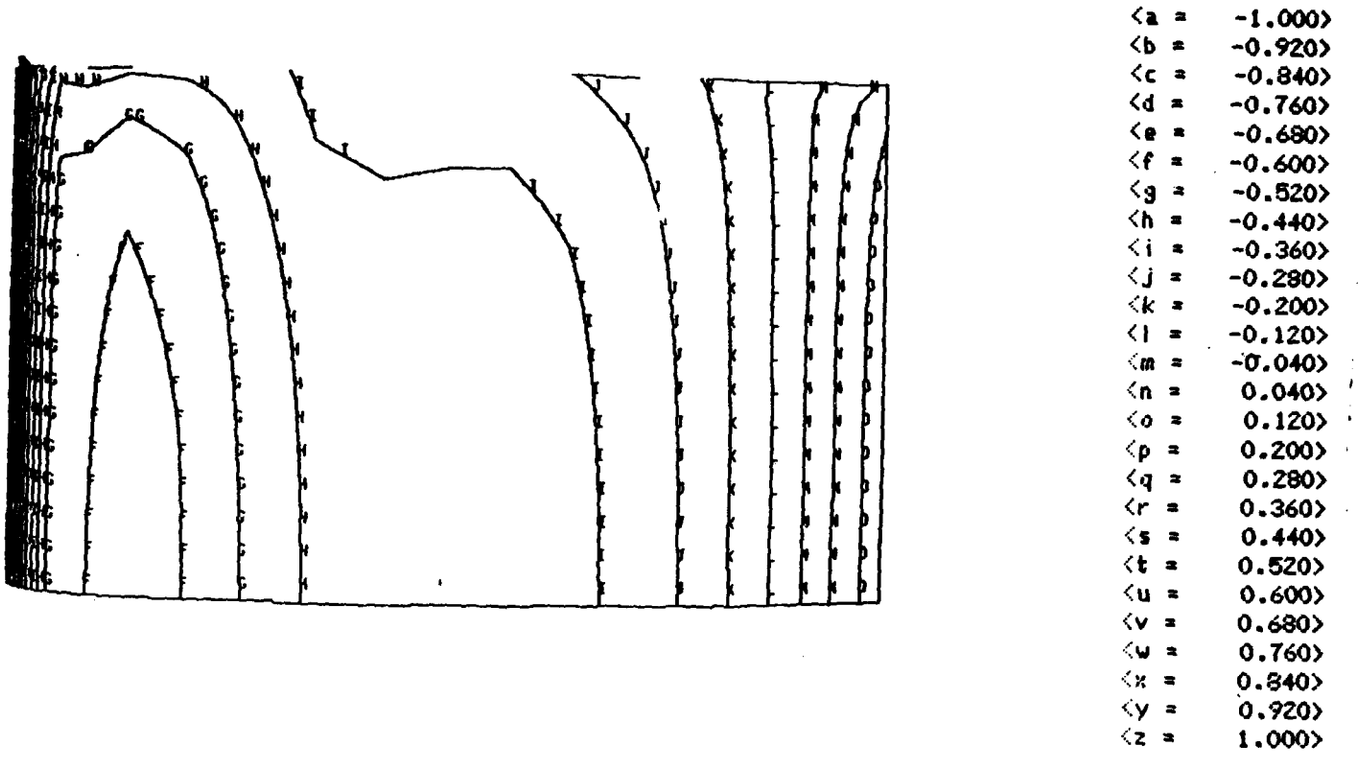

Fig. 13b. C_p contours on the sail surface, sail and large strut.

Fig. 13. (Continued)

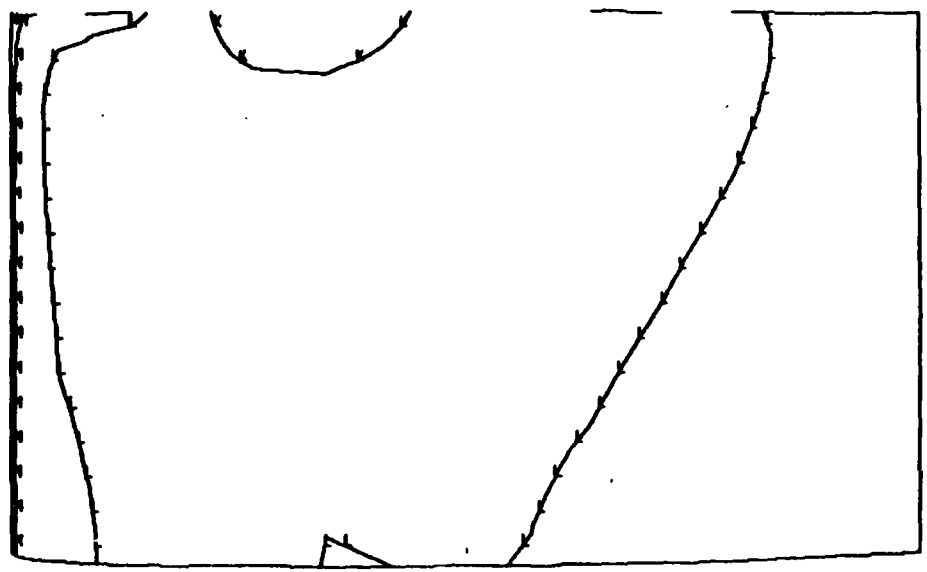

Fig. 13c. ΔC_p contours on the sail surface.

Fig. 13. (Continued)

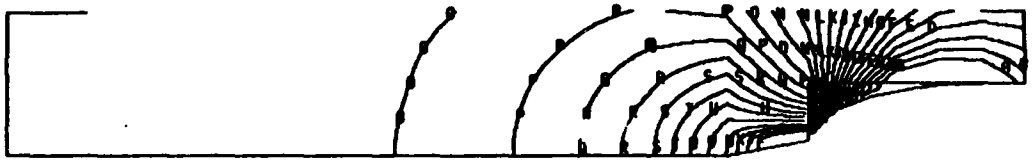

Fig. 13d. C_p contours on the hull surface, sail and large strut.

Fig. 13. (Continued)

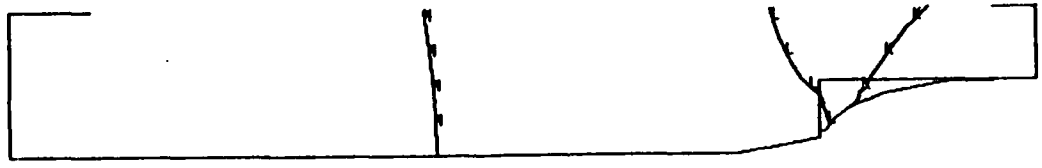

Fig. 13e. ΔC_p contours on the hull surface.

Fig. 13. (Continued)

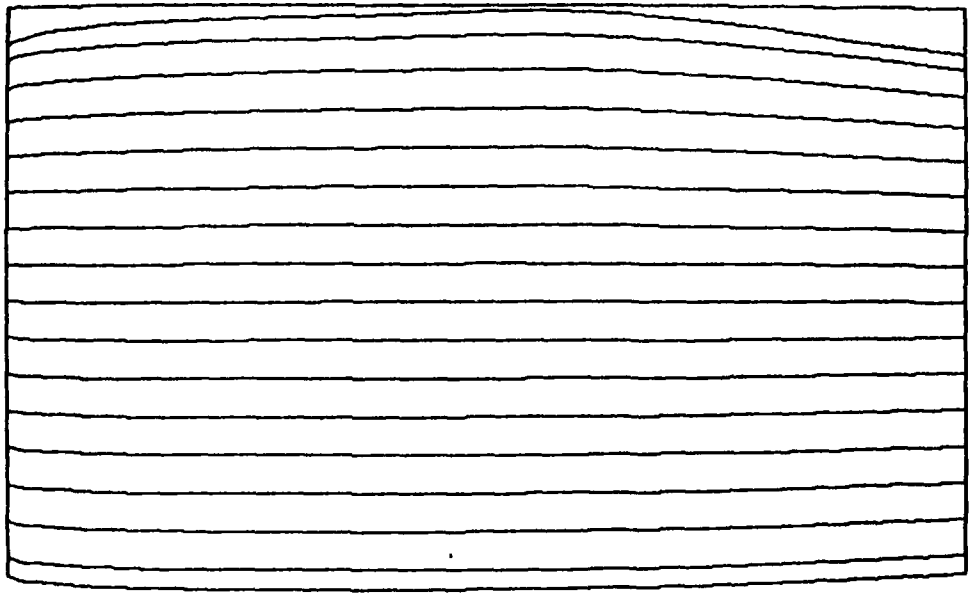

Fig. 14a. Streamlines on the sail surface, sail and large strut.

Fig. 14. Streamlines and pressure contours for the SSN 688 with suction and blowing applied to the strut section.

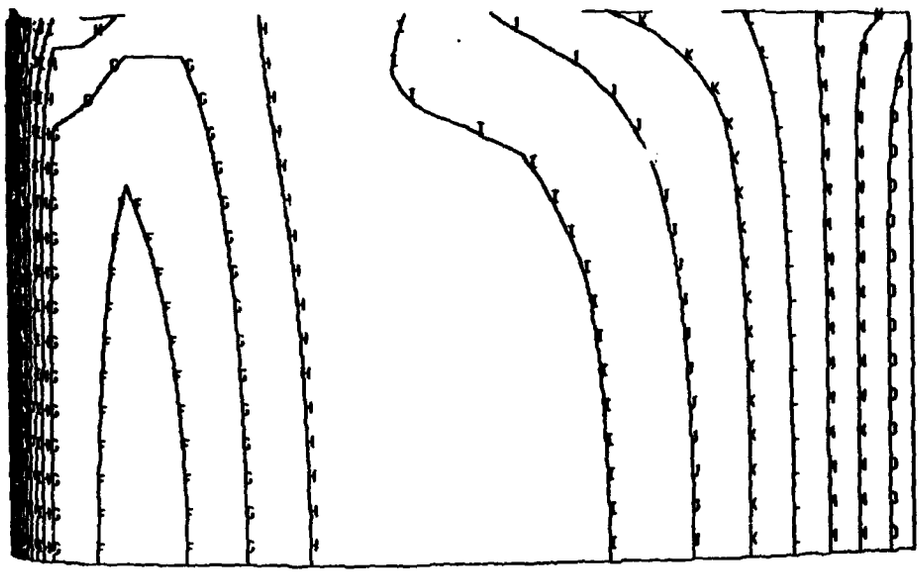

<a = -1.000>
<b = -0.920>
<c = -0.840>
<d = -0.760>
<e = -0.680>
<f = -0.600>
<g = -0.520>
<h = -0.440>
<i = -0.360>
<j = -0.280>
<k = -0.200>
<l = -0.120>
<m = -0.040>
<n = 0.040>
<o = 0.120>
<p = 0.200>
<q = 0.280>
<r = 0.360>
<s = 0.440>
<t = 0.520>
<u = 0.600>
<v = 0.680>
<w = 0.760>
<x = 0.840>
<y = 0.920>
<z = 1.000>

Fig. 14b. C_p contours on the sail surface, sail and large strut.

Fig. 14. (Continued)

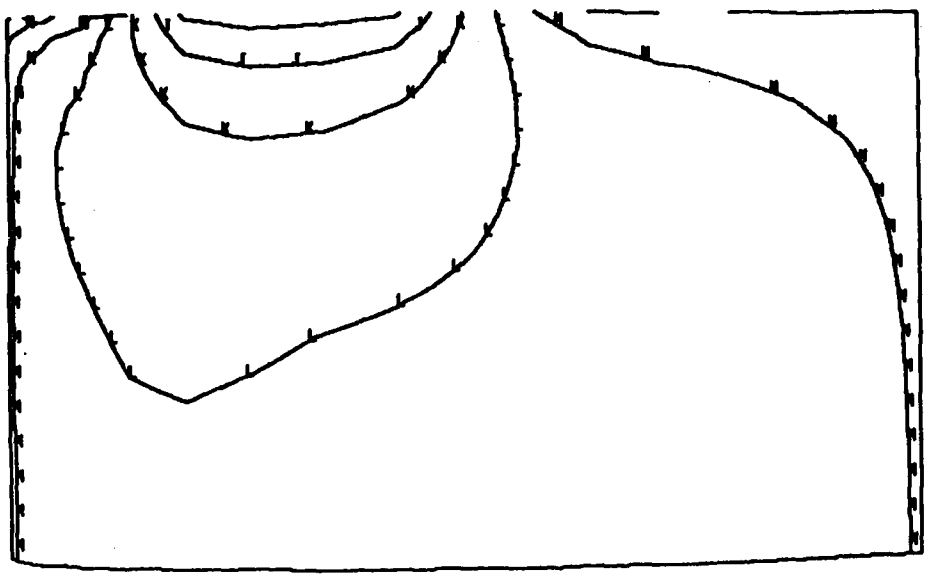

<a = -0.400>
<b = -0.368>
<c = -0.336>
<d = -0.304>
<e = -0.272>
<f = -0.240>
<g = -0.208>
<h = -0.176>
<i = -0.144>
<j = -0.112>
<k = -0.080>
<l = -0.048>
<m = -0.016>
<n = 0.016>
<o = 0.048>
<p = 0.080>
<q = 0.112>
<r = 0.144>
<s = 0.176>
<t = 0.208>
<u = 0.240>
<v = 0.272>
<w = 0.304>
<x = 0.336>
<y = 0.368>
<z = 0.400>

Fig. 14c. ΔC_p contours on the sail surface.

Fig. 14. (Continued)

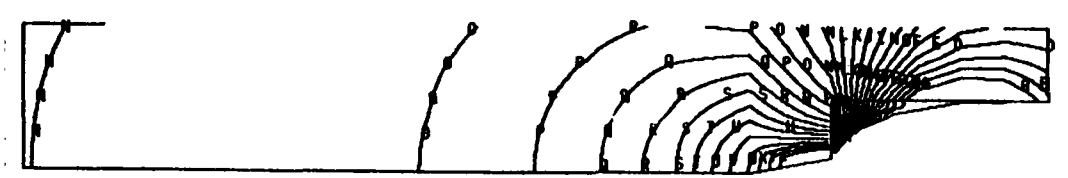

Fig. 14d. C_p contours on the hull surface, sail and large strut.

Fig. 14. (Continued)

Fig. 14e. ΔC_p contours on the hull surface.

Fig. 14. (Continued)

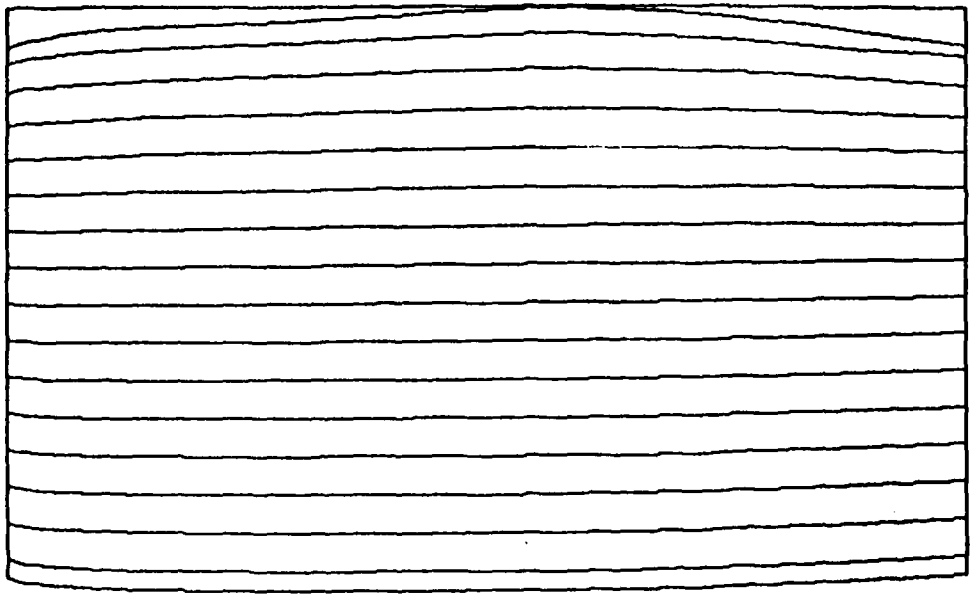

Fig. 15a. Streamlines on the sail surface, sail and large strut.

Fig. 15. Streamlines and pressure contours for the SSN 688 with suction applied to the strut section.

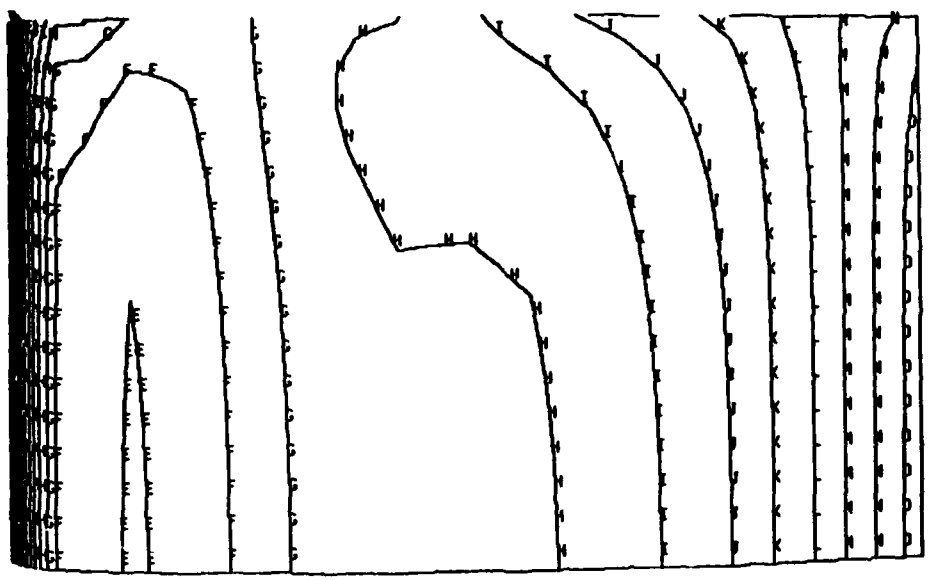

<a = -1.000>
<b = -0.920>
<c = -0.840>
<d = -0.760>
<e = -0.680>
<f = -0.600>
<g = -0.520>
<h = -0.440>
<i = -0.360>
<j = -0.280>
<k = -0.200>
<l = -0.120>
<m = -0.040>
<n = 0.040>
<o = 0.120>
<p = 0.200>
<q = 0.280>
<r = 0.360>
<s = 0.440>
<t = 0.520>
<u = 0.600>
<v = 0.680>
<w = 0.760>
<x = 0.840>
<y = 0.920>
<z = 1.000>

Fig. 15b. C_p contours on the sail surface, sail and large strut.

Fig. 15. (Continued)

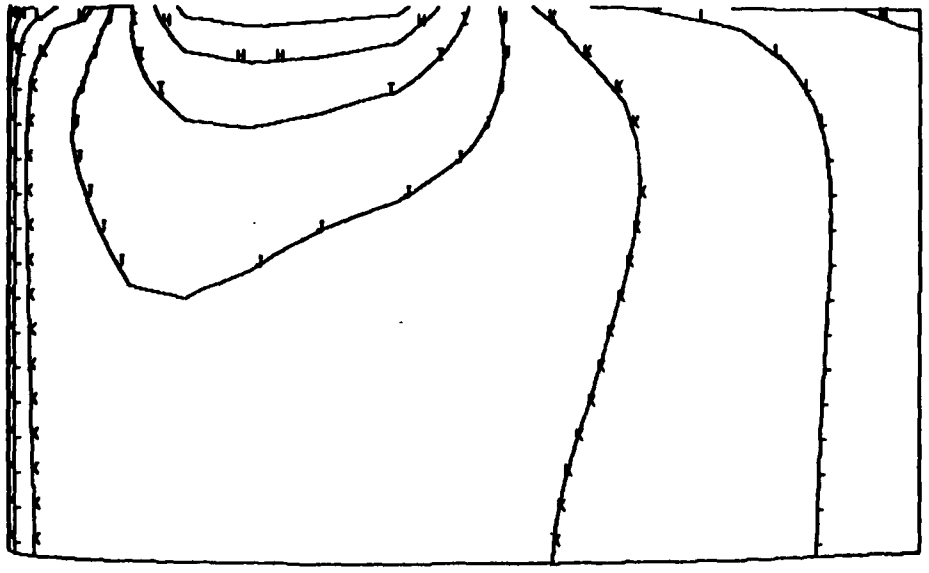

Fig. 15c. ΔC_p contours on the sail surface.

Fig. 15. (Continued)

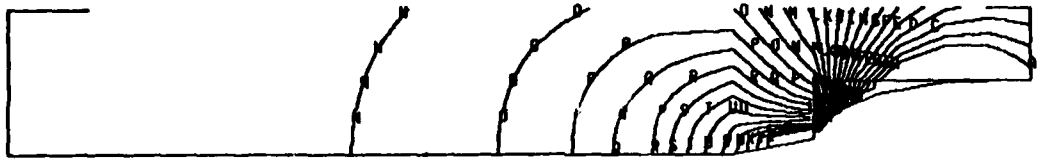

Fig. 15d. C_p contours on the hull surface, sail and large strut.

Fig. 15. (Continued)

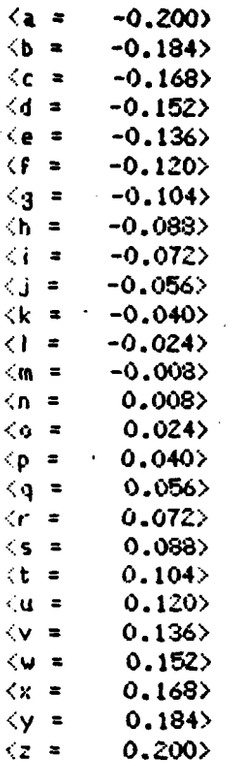

Fig. 15e. ΔC_p contours on the hull surface.

Fig. 15. (Continued)

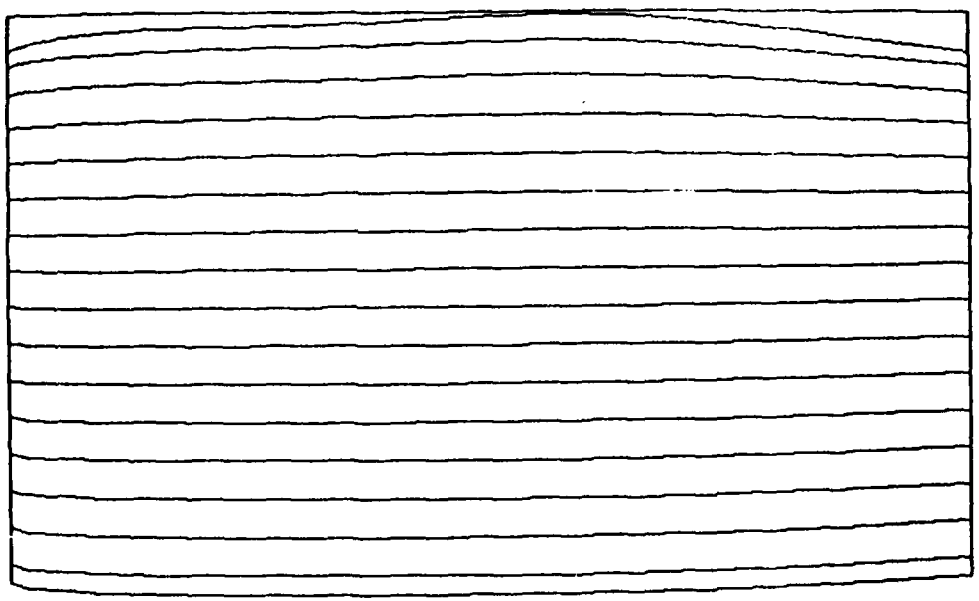

Fig. 16a. Streamlines on the sail surface, sail and large strut.

Fig. 16. Streamlines and pressure contours for the SSN 688 with suction applied to the strut cap section.

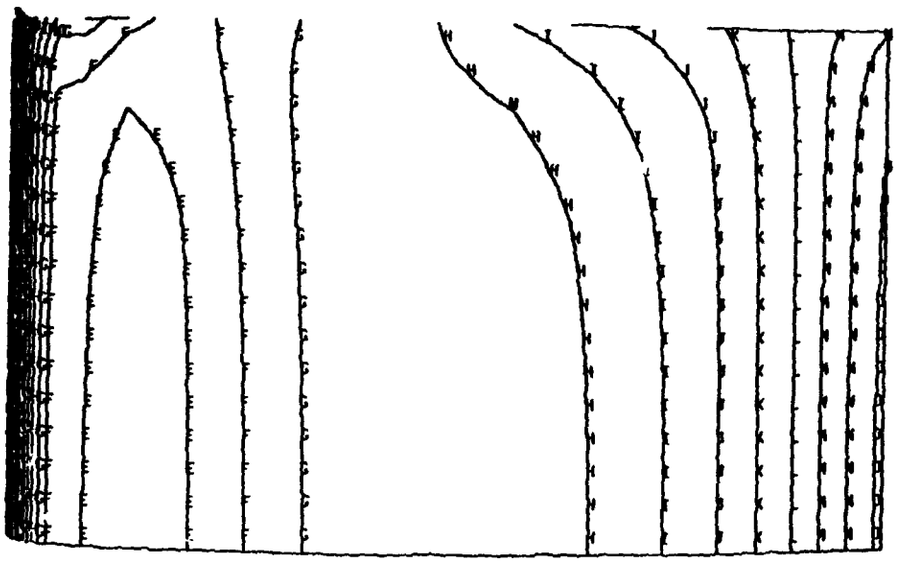

<a = -1.000>
<b = -0.920>
<c = -0.840>
<d = -0.760>
<e = -0.680>
<f = -0.600>
<g = -0.520>
<h = -0.440>
<i = -0.360>
<j = -0.280>
<k = -0.200>
<l = -0.120>
<m = -0.040>
<n = 0.040>
<o = 0.120>
<p = 0.200>
<q = 0.280>
<r = 0.360>
<s = 0.440>
<t = 0.520>
<u = 0.600>
<v = 0.680>
<w = 0.760>
<x = 0.840>
<y = 0.920>
<z = 1.000>

Fig. 16b. C_p contours on the sail surface, sail and large strut.

Fig. 16. (Continued)

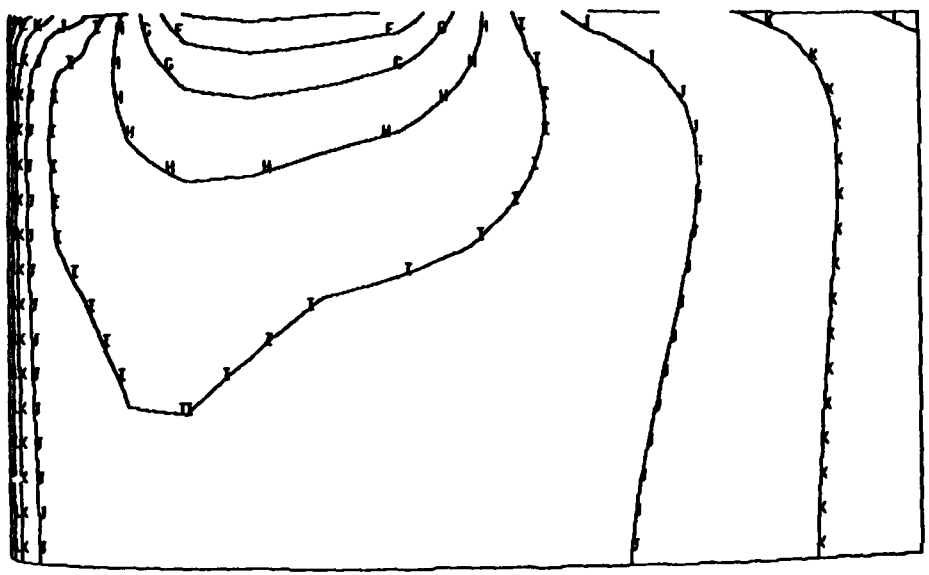

<a = -0.400>
<b = -0.368>
<c = -0.336>
<d = -0.304>
<e = -0.272>
<f = -0.240>
<g = -0.208>
<h = -0.176>
<i = -0.144>
<j = -0.112>
<k = -0.080>
<l = -0.048>
<m = -0.016>
<n = 0.016>
<o = 0.048>
<p = 0.080>
<q = 0.112>
<r = 0.144>
<s = 0.176>
<t = 0.208>
<u = 0.240>
<v = 0.272>
<w = 0.304>
<x = 0.336>
<y = 0.368>
<z = 0.400>

Fig. 16c. ΔC_p contours on the sail surface.

Fig. 16. (Continued)

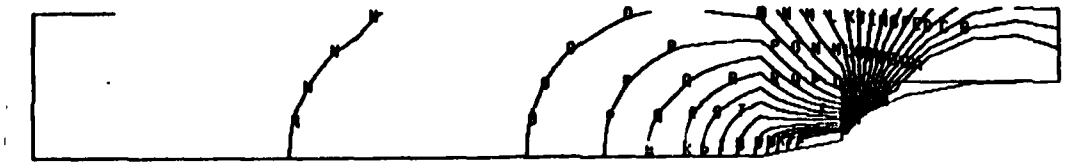

Fig. 16d. C_p contours on the hull surface, sail and large strut.

Fig. 16. (Continued)

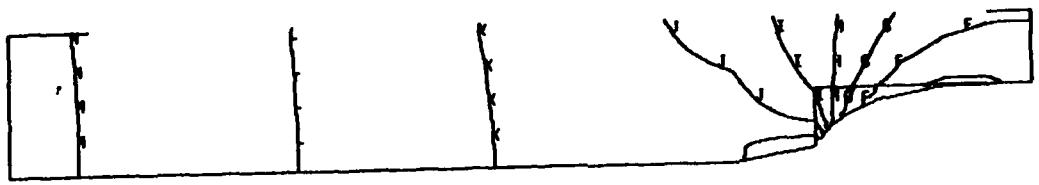

<a = -0.200>
<b = -0.184>
<c = -0.168>
<d = -0.152>
<e = -0.136>
<f = -0.120>
<g = -0.104>
<h = -0.088>
<i = -0.072>
<j = -0.056>
<k = -0.040>
<l = -0.024>
<m = -0.008>
<n = 0.008>
<o = 0.024>
<p = 0.040>
<q = 0.056>
<r = 0.072>
<s = 0.088>
<t = 0.104>
<u = 0.120>
<v = 0.136>
<w = 0.152>
<x = 0.168>
<y = 0.184>
<z = 0.200>

Fig. 16e. ΔC_p contours on the hull surface.

Fig. 16. (Continued)

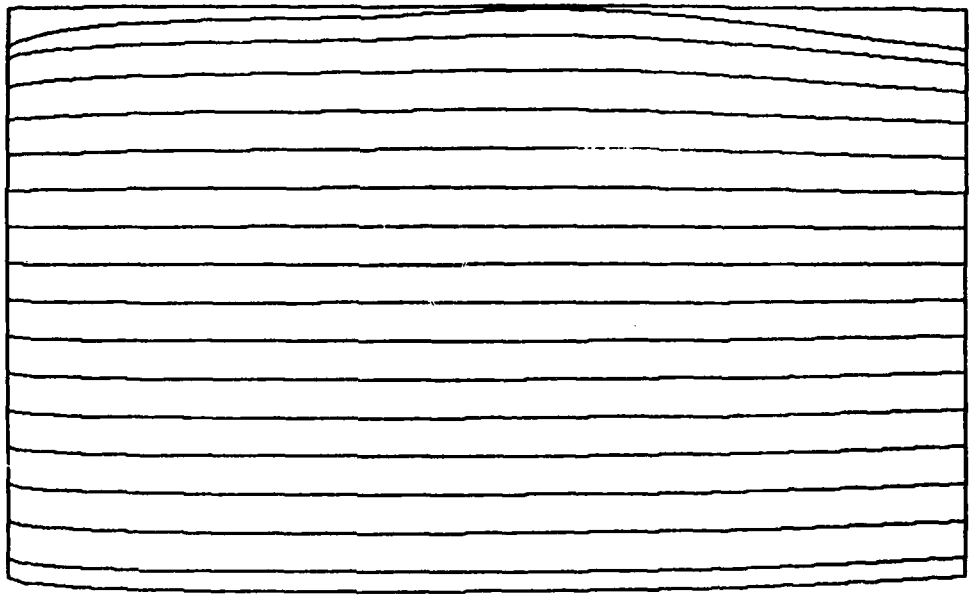

Fig. 17a. Streamlines on the sail surface, sail and large strut.

Fig. 17. Streamlines and pressure contours for the SSN 688 with suction applied to the sail cap section.

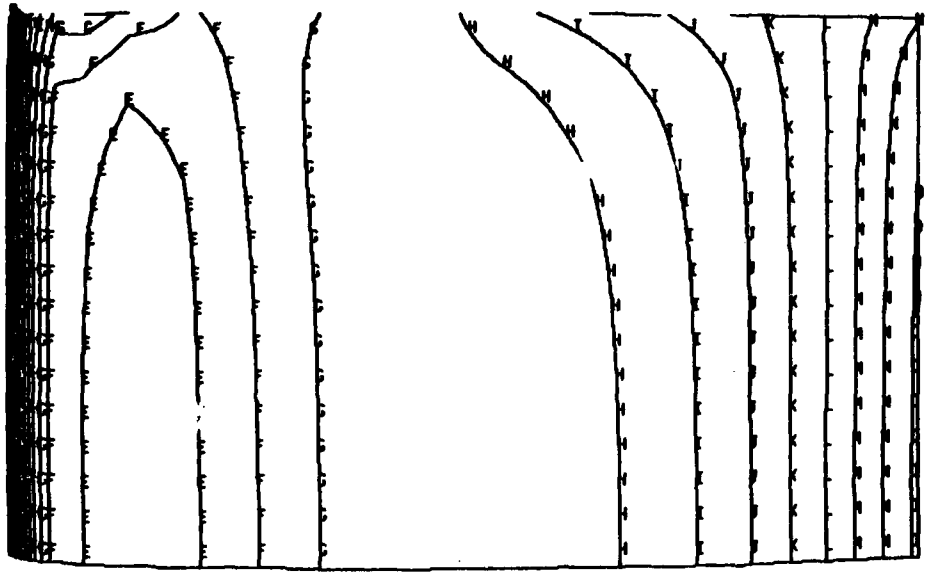

<a = -1.000>
<b = -0.920>
<c = -0.840>
<d = -0.760>
<e = -0.680>
<f = -0.600>
<g = -0.520>
<h = -0.440>
<i = -0.360>
<j = -0.280>
<k = -0.200>
<l = -0.120>
<m = -0.040>
<n = 0.040>
<o = 0.120>
<p = 0.200>
<q = 0.280>
<r = 0.360>
<s = 0.440>
<t = 0.520>
<u = 0.600>
<v = 0.680>
<w = 0.760>
<x = 0.840>
<y = 0.920>
<z = 1.000>

Fig. 17b. C_p contours on the sail surface, sail and large strut.

Fig. 17. (Continued)

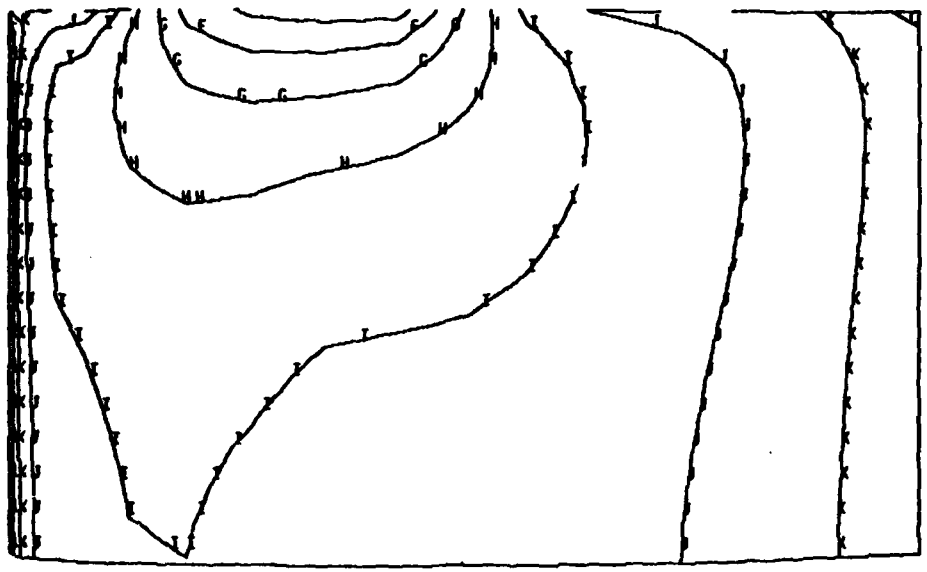

<a = -0.400>
<b = -0.368>
<c = -0.336>
<d = -0.304>
<e = -0.272>
<f = -0.240>
<g = -0.208>
<h = -0.176>
<i = -0.144>
<j = -0.112>
<k = -0.080>
<l = -0.048>
<m = -0.016>
<n = 0.016>
<o = 0.048>
<p = 0.080>
<q = 0.112>
<r = 0.144>
<s = 0.176>
<t = 0.208>
<u = 0.240>
<v = 0.272>
<w = 0.304>
<x = 0.336>
<y = 0.368>
<z = 0.400>

Fig. 17c. ΔC_p contours on the sail surface.

Fig. 17. (Continued)

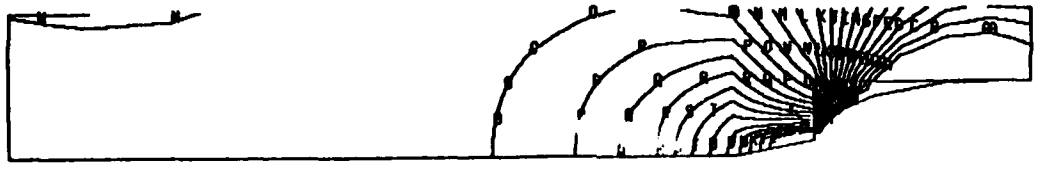

Fig. 17d. C_p contours on the hull surface, sail and large strut.

Fig. 17. (Continued)

Fig. 17e. ΔC_p contours on the hull surface.

Fig. 17. (Continued)

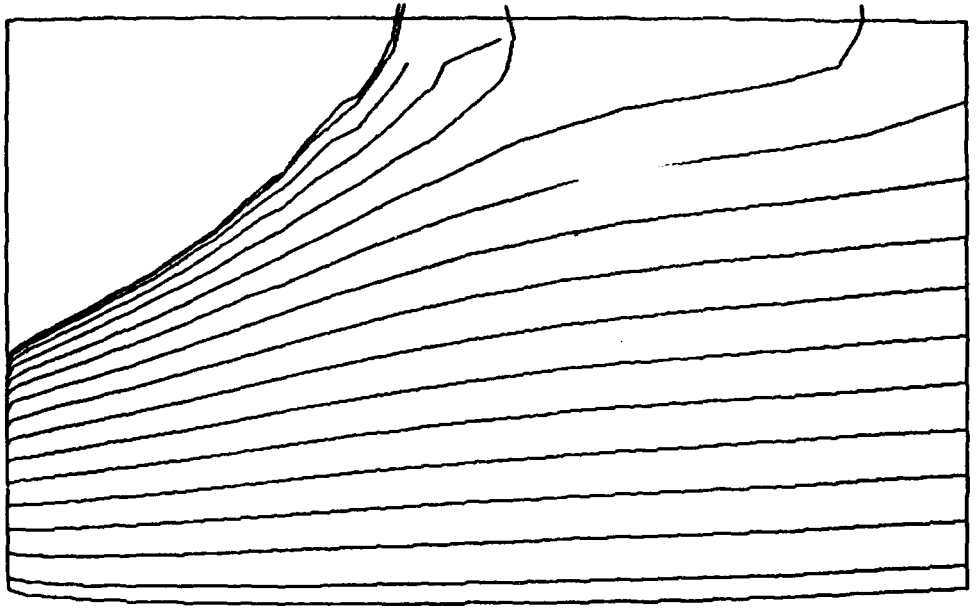

Fig. 18a. Streamlines on the sail surface, sail and large strut.

Fig. 18. Streamlines and pressure contours for the SSN 688 with increased suction applied to the sail cap section.

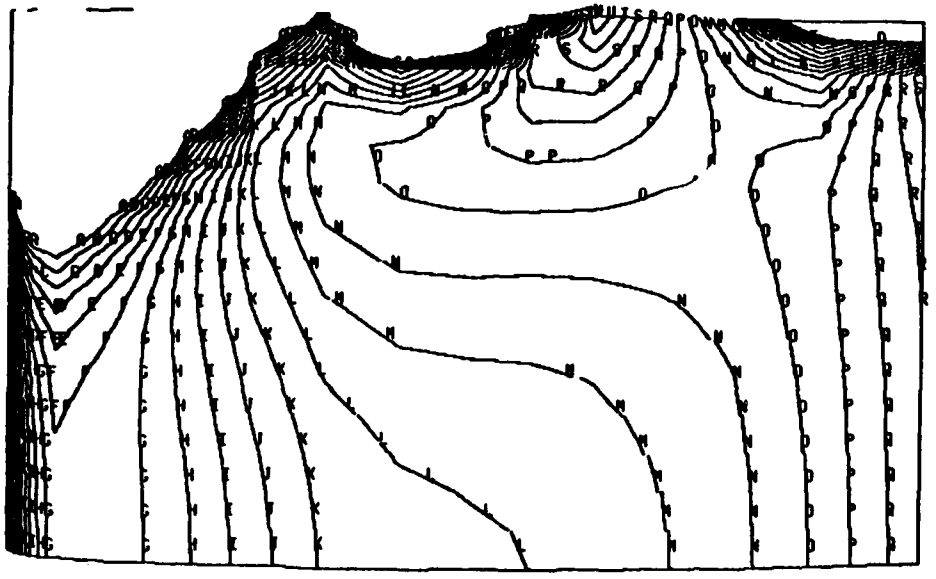

<a = -1.000>
<b = -0.920>
<c = -0.840>
<d = -0.760>
<e = -0.680>
<f = -0.600>
<g = -0.520>
<h = -0.440>
<i = -0.360>
<j = -0.280>
<k = -0.200>
<l = -0.120>
<m = -0.040>
<n = 0.040>
<o = 0.120>
<p = 0.200>
<q = 0.280>
<r = 0.360>
<s = 0.440>
<t = 0.520>
<u = 0.600>
<v = 0.680>
<w = 0.760>
<x = 0.840>
<y = 0.920>
<z = 1.000>

Fig. 18b. C_p contours on the sail surface, sail and large strut.

Fig. 18. (Continued)

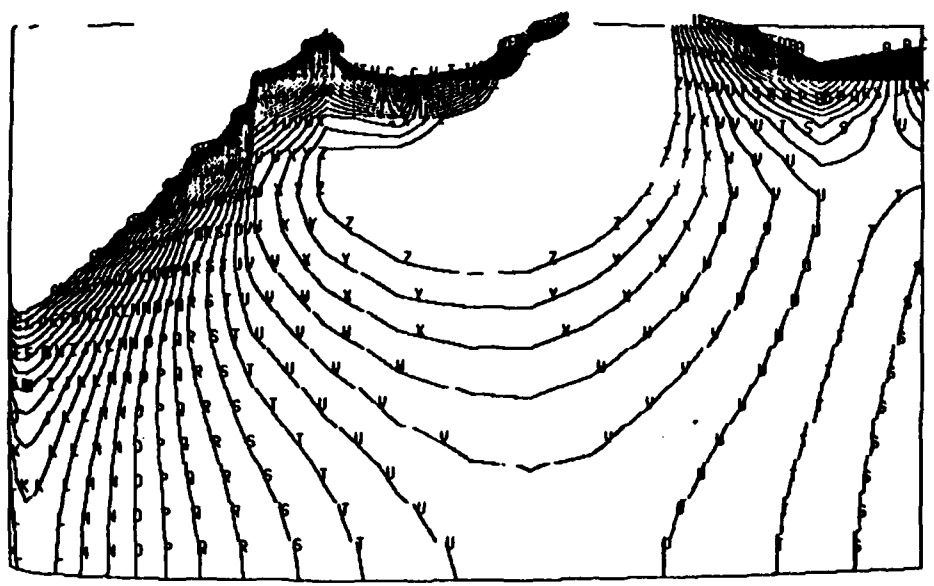

Fig. 18c. ΔC_p contours on the sail surface.

Fig. 18. (Continued)

Fig. 18d. C_p contours on the hull surface, sail and large strut.

Fig. 18. (Continued)

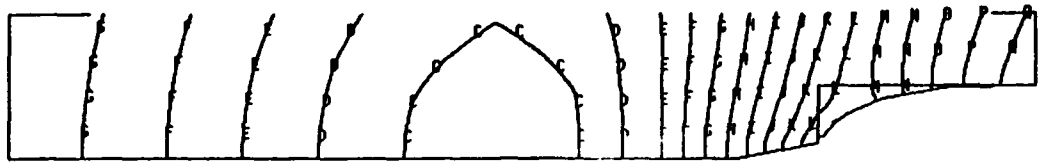

Fig. 18e. ΔC_p contours on the hull surface.

Fig. 18. (Continued)

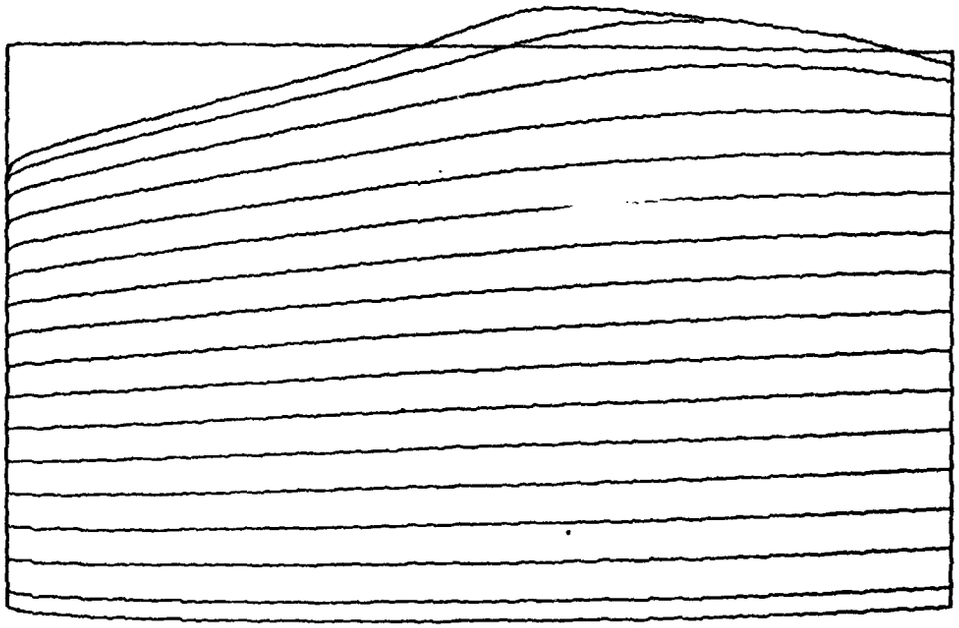

Fig. 19a. Streamlines on the sail surface, sail and large strut.

Fig. 19. Streamlines and pressure contours for the SSN 688 with increased suction applied to the strut cap section.

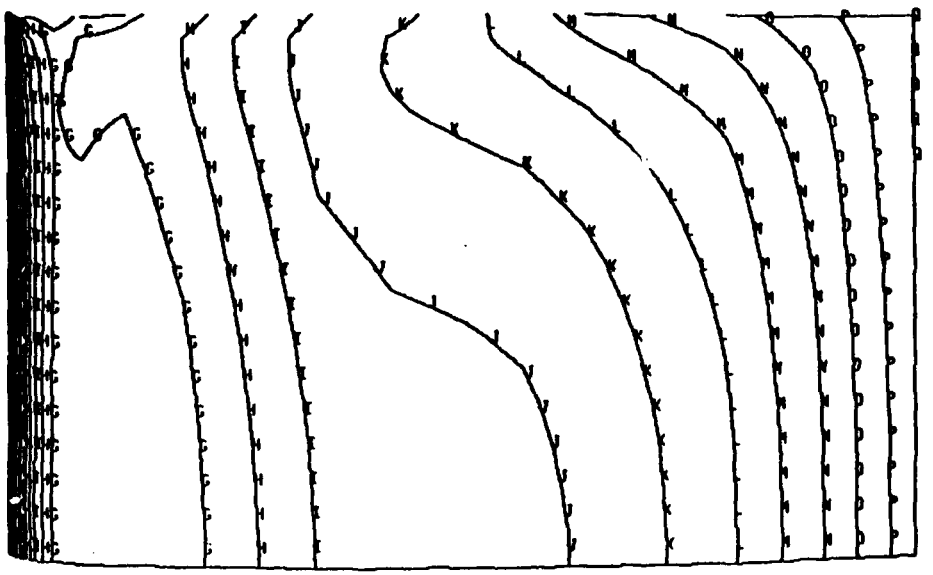

<a = -1.000>
<b = -0.920>
<c = -0.840>
<d = -0.760>
<e = -0.680>
<f = -0.600>
<g = -0.520>
<h = -0.440>
<i = -0.360>
<j = -0.280>
<k = -0.200>
<l = -0.120>
<m = -0.040>
<n = 0.040>
<o = 0.120>
<p = 0.200>
<q = 0.280>
<r = 0.360>
<s = 0.440>
<t = 0.520>
<u = 0.600>
<v = 0.680>
<w = 0.760>
<x = 0.840>
<y = 0.920>
<z = 1.000>

Fig. 19b. C_p contours on the sail surface, sail and large strut.

Fig. 19. (Continued)

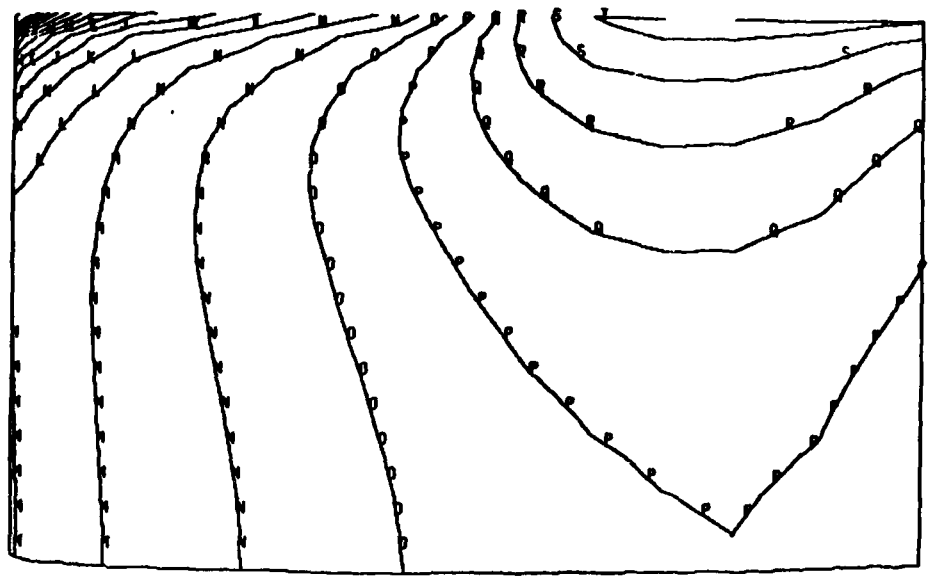

<a = -0.400>
<b = -0.368>
<c = -0.336>
<d = -0.304>
<e = -0.272>
<f = -0.240>
<g = -0.208>
<h = -0.176>
<i = -0.144>
<j = -0.112>
<k = -0.080>
<l = -0.048>
<m = -0.016>
<n = 0.016>
<o = 0.048>
<p = 0.080>
<q = 0.112>
<r = 0.144>
<s = 0.176>
<t = 0.208>
<u = 0.240>
<v = 0.272>
<w = 0.304>
<x = 0.336>
<y = 0.368>
<z = 0.400>

Fig. 19c. ΔC_p contours on the sail surface.

Fig. 19. (Continued)

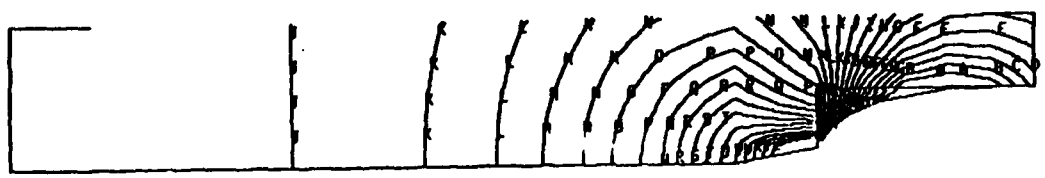

Fig. 19d. C_p contours on the hull surface, sail and large strut.

Fig. 19. (Continued)

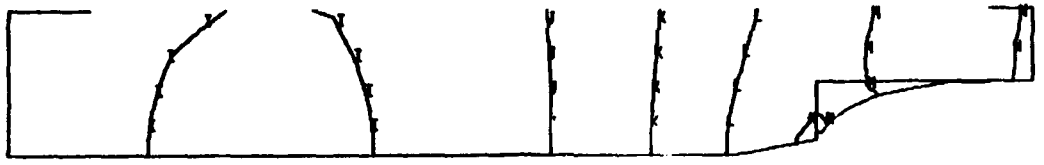

Fig. 19e. ΔC_p contours on the hull surface.

Fig. 19. (Continued)

REFERENCES

1. Lighthill, M. J., Laminar Boundary Layers, Oxford University Press, Amen London E.C.4 (1963).
2. Hess J.L., Smith A.M.O., "Calculation of Nonlifting Potential Flow About Arbitrary Three Dimensional Bodies", Douglas Aircraft Company Rept. ES40622 (1962).
3. Holt D.R., Hunt B., "Use of Panel Methods for the Evaluation of Subsonic Wall Interference", British Aerospace (Aircraft Group), AGARD (1982).
4. Dawson, C.W., Dean, J.S., "The XYZ Potential Flow Program", DTNSRDC Rept. 3892 (1972).